IEEE Access
Multidisciplinary | Rapid Review | Open Access Journal

Received 31 January 2024, accepted 27 March 2024, date of publication 18 April 2024, date of current version 7 May 2024.

Digital Object Identifier 10.1109/ACCESS.2024.3390566

RESEARCH ARTICLE

ExoventQ: A Novel Low-Cost Portable Negative Pressure Ventilator Design and Implementation

SHAHD SAMEER MOHAMMED GABEN[1], NADA ABUGHANAM[1], NABIL IBTEHAZ[2], SAKIB MAHMUD[1], (Member, IEEE), GHADA AL NOAIMI[1], ABDULRAHMAN ALQAHTANI[3,4], AMITH KHANDAKAR[1], (Senior Member, IEEE), AND MUHAMMAD E. H. CHOWDHURY[1], (Senior Member, IEEE)

[1]Department of Electrical Engineering, Qatar University, Doha, Qatar
[2]Department of Computer Science, Purdue University, West Lafayette, IN 47907, USA
[3]Department of Biomedical Technology, College of Applied Medical Sciences in Al-Kharj, Prince Sattam Bin Abdulaziz University, Al-Kharj 11942, Saudi Arabia
[4]Department of Medical Equipment Technology, College of Applied Medical Sciences, Majmaah University, Al Majma'ah 11952, Saudi Arabia

Corresponding author: Muhammad E. H. Chowdhury (mchowdhury@qu.edu.qa)

This work was supported in part by Qatar University Student Grant QUST-1-CENG-2023-796, and in part by Prince Sattam Bin Abdulaziz University under Project PSAU/2024/R/1445.

ABSTRACT The emergence of COVID-19 resulted in significant shortages of mechanical ventilators globally. This prompted investigations into developing new, cost-effective methods for producing ventilators. Different types of ventilators, such as positive pressure ventilators (PPVs), conventional negative pressure ventilators (NPVs), and biphasic cuirass ventilators (BCVs), were considered. However, PPVs were found to pose health risks and were expensive to manufacture. Thus, this study introduces ExoventQ, an innovative respiratory support device inspired by traditional NPV designs. ExoventQ was meticulously designed, simulated, implemented, and tested in two modes: continuous negative extrathoracic pressure (CNEP) and cyclic negative pressure ventilation (CNPV). It consists of three main components: a pressure vessel, a pumping system, and a control panel. Each component was designed with attention to pressure distribution, material, safety, cost, and portability. Through ANSYS stress analysis, ExoventQ was developed with a squircle-shaped polycarbonate vessel capable of withstanding up to 50 millibar (mbar) of vacuum pressure. This design also prevents airway tilting when placed on its side, providing more comfort for the patient. Pressure regulation inside the vessel is achieved through a bypass butterfly valve controlled by a servo motor. The user interface is implemented on a Raspberry Pi touchscreen, enabling input through rotating knobs and displaying output for monitoring. Safety measures include audio and visual alarms, along with a power switch that halts ventilation if the vacuum in the vessel drops below 40 mbar. The successful design and implementation of ExoventQ have the potential to enable mass production of safe and affordable NPVs to address pulmonary complications.

INDEX TERMS ExoventQ, ventilators, negative pressure ventilator (NPV), pulmonary diseases, COVID-19.

I. INTRODUCTION

Each year, millions of individuals are affected by lung disorders, including Chronic Obstructive Pulmonary Disease (COPD), which alone accounts for 3 million deaths annually. Additionally, 4 million lives are lost due to lower respiratory tract infections, and 1.6 million deaths are attributed to lung cancer [1]. These patients require specialized medical equipment, such as ventilators, to support their respiratory function during recovery. Moreover, challenging situations like wars, natural disasters, and pandemics often result in a significant number of victims needing lung ventilation for

The associate editor coordinating the review of this manuscript and approving it for publication was Janmenjoy Nayak.

survival. Consequently, the availability of ventilators and skilled experts becomes critical in preparedness for such scenarios. In the 1950s, at the onset of the polio pandemic, there was a severe shortage of ventilators, which prompted the development of a new ventilation method known as Positive Pressure Ventilation (PPV) [2]. More recently, the COVID-19 pandemic recorded millions of cases requiring hundreds of thousands of ventilators [3]. While COVID-19 clearly had significant effects on patients' physical, mental [4], and social health [4], its clinical impact was immense. Patients with COVID-19 and similar respiratory illnesses often experience alveolar damage and lung fibrosis, leading to reduced blood oxygen saturation and necessitating acute mechanical ventilator (MV) support [5]. During the peak of the COVID-19 outbreak, the Center for Disease Control and Prevention (CDC) [6] emphasized the urgent need for rapid mass production of ventilators to address the supply shortage [7]. This was necessary since many of the available ventilators were already in use by patients with other respiratory disorders.

Negative Pressure Ventilators (NPVs) were prevalent in the 19th and early 20th centuries. The initial types to be implemented included tank ventilators, followed by negative pressure chambers, raincoat ventilators, and cuirass ventilators. However, it was the invention of the iron lung [8] that truly made NPVs a clinical reality. Drinker et al. [8] were responsible for its original design and construction, while Bause et al. [9] oversaw its manufacturing and sales. The utility of the iron lung reached its zenith in the 1930s and extended into the 1960s during the poliomyelitis epidemic when thousands of people required parallel ventilation [10], [11], [12]. However, this popularity was short-lived, especially after the end of the polio epidemic [10]. That era witnessed a high demand for ventilators and faced a scarcity of iron lungs, leading to the introduction of Positive Pressure Ventilators (PPVs), also known as Intensive Care Unit (ICU) ventilators [10]. Mass production of PPVs became successful as they provided artificial respiration by applying positive pressure to the airways. At the end of World War II, small and compact Intermittent Positive Pressure Breathing Machines (IPPBs) were developed, such as the Bennett and Bird IPPB machines [13]. From that point until today, hospitals and medical care units have relied predominantly on PPVs [14], [15]. These machines offer various features and modes for Noninvasive PPV (NIPPV), using facial or nasal masks, or Invasive PPV (IPPV), employing Endotracheal Tubes (ETT) or Tracheostomy Tubes (TT). However, PPVs, especially IPPVs, can impose serious health complications due to factors related to intubation, sedation, and PPV management [16].

Although the production of PPVs continues and is primarily used for respiratory care worldwide, both its non-invasive and invasive techniques have many associated complications, including decreased cardiac output, unintended acute respiratory alkalosis, increased intracranial pressure, meteorism (massive gastric distension), and impaired hepatic and renal function. The most severe PPV-related complications that could lead to mortality include pneumothorax, bronchopleural fistula, nosocomial pneumonia, as well as barotrauma and volutrauma [17]. These complications led to the development of what is now known as Biphasic Cuirass Ventilators (BCVs) [18], a type of External High-Frequency Oscillator (EHFO) [19] that utilizes a shell-like chest enclosure to apply extra-thoracic pressure. High-Frequency Ventilation (HFV) was initially introduced in the 1970s to mitigate or prevent the complications associated with PPVs. HFV refers to a ventilation technique that employs a significantly higher respiratory rate than normal breathing, with lower tidal volumes and peak pressure requirements compared to PPV [20]. HFV encompasses three types of high-frequency ventilation: High-Frequency Positive Pressure Ventilation (HFPPV), high-frequency jet Ventilation (HFJV), and the most common High-Frequency Oscillatory Ventilation (HFOV) [21]. Although HFOV is more lung-protective and demonstrates greater lung recruitment than conventional PPVs, as observed in clinical trials, it introduced its own set of complications [22]. These complications include an elevated risk of barotrauma, pneumothorax, endotracheal tube obstruction, and hemodynamic compromise [23], [24].

In recent years, mechanical ventilators (MVs) have been widely employed in clinical facilities worldwide to support patients with a diverse range of complexities. In addition to addressing lung diseases such as COPD, pulmonary edema [19], or Acute Respiratory Distress Syndrome (ARDS) [17], [21], MVs have also found utility in resuscitating patients afflicted with neuromuscular diseases [25], cardiopulmonary arrest [26], and diabetes mellitus (DM) [27]. In various medical fields, newer techniques have been incorporated or innovated to replace or enhance existing MV-based systems, aiming to create more focused, domain-oriented clinical solutions. For example, recent findings indicate that, when compared with Positive Inspiratory Pressure (PIP) or tidal volume-targeted modes, proportional assist ventilation with Apnea back-up is more suitable for neonates with moderate lung diseases [28]. Moreover, several studies have been conducted to enhance the pressure and/or volume controls of mechanical ventilators (MVs), ensuring improved respiratory support during emergencies [29]. Nevertheless, the most extensively studied limitation of existing ventilators is their invasiveness, which contributed to a significant number of deaths during the peak of the COVID-19 pandemic [30]. This circumstance prompted the exploration of non-invasive solutions [31]. The prolonged use of invasive MVs often leads to respiratory tract complications such as Ventilator-Associated Pneumonia (VAP) [32]. To address such challenges, researchers have proposed various non-MV solutions, including Extracorporeal Membrane Oxygenation (ECMO) and subsequent carbon dioxide removal [33], [34], [35], in addition to non-invasive MV solutions.

Speaking of COVID-19, it resulted in a severe shortage of ventilators, a situation reminiscent of past pandemics. Recent

studies have shown a close link between deaths resulting from extended ICU stays and ventilator-induced pneumonia [36]. Even during the COVID-19 pandemic, the death of many patients has been linked to the pneumonia caused by currently abundant positive pressure MVs [37]. Given the high demand for ventilators and their components during similar pandemics, it is imperative to explore alternative methods early for creating safe but cost-effective and easily producible ventilator systems. Abboudi et al. [24] introduced an emergency ventilator design based on an Arduino microcontroller, which controls a stepper motor and incorporates sensors for monitoring pressure, body temperature, and pulse oximetry. This design eliminates the need for human intervention in compressing the bag by employing a lever mechanism and is equipped to trigger facility alarms in the event of detected abnormalities. In a separate effort, Christou et al. [38] developed and implemented an emergency ventilator known as ''GlasVent,'' an automated adaptation of a manual resuscitator device. GlasVent employs 3D-printed mechanical components, readily available materials, and off-the-shelf electronic and sensing devices, enabling quick assembly. However, it should be noted that GlasVent lacks a safety control system for setting alarms and operates on a PPV. MADvent, developed by Vasan et al. [39], was a PPV-based emergency solution designed to alleviate the excessive pressure on the global ventilator supply chain during the COVID-19 pandemic.

Based on the above discussion, this paper aims to develop **ExoventQ**, an NPV designed to meet medical requirements while adhering to relevant constraints and standards (such as ISO 19223:2019 for Lung ventilators and related equipment - Vocabulary and semantics [40], Ventilation Standards for Use in Artificial Respiration [41], and TotalCare Bed used in Hamad Medical Standards for Anthropometry Assessment [42]). NPVs offer an alternative approach, providing care and relief to patients without competing with the existing PPV industry. Furthermore, NPVs inherently offer a safer option compared to PPVs by avoiding the complexities associated with intubation. Thus, the proposed ventilator design is innovative, safe, cost-effective, portable, and adaptable for diverse clinical scenarios. The primary contributions of this study can be summarized as follows:

- The design and implementation of a ventilator that prioritizes patient safety and comfort while accommodating different pressure levels.
- The development and integration of a robust pressure control system for the ventilator, suitable for ventilating patients in various medical situations.
- The creation of a user-friendly interface enables medical professionals to control and monitor multiple parameters, including inspiration pressure, expiration pressure, respiratory rate, and inspiration-to-expiration (I:E) ratio.

The remainder of the manuscript is structured as follows: Section II offers a brief overview of pulmonary ventilation. Section III elucidates fundamental concepts essential for designing **ExoventQ**. It also provides an illustration and an overview of the system's design, characterization, and concept of operation. In Section IV, we present and analyze both the quantitative and qualitative outcomes obtained from various components of the proposed system. Section V includes concluding remarks, outlines the system's limitations, and explores potential avenues for future research in this field.

II. PULMONARY VENTILATION

Pulmonary ventilation is the scientific term that describes the natural act of breathing. Pulmonary ventilation consists of two phases viz. inspiration and expiration [43]. Inspiration entails drawing air into the lungs, while expiration involves expelling air from the lungs. A complete cycle of inspiration and expiration constitutes a respiratory cycle. The respiration process is driven by the pressure differential between the external environment (atmospheric pressure, denoted as $\boldsymbol{P_{atm}}$) and the interior of the lungs (alveolar pressure, $\boldsymbol{P_{alv}}$, and intrapleural pressure, $\boldsymbol{P_{ip}}$). In this context, the standard reference is $\boldsymbol{P_{atm}}$. Consequently, pressure values below $\boldsymbol{P_{atm}}$ are considered negative, those above $\boldsymbol{P_{atm}}$ are regarded as positive, and pressure equal to $\boldsymbol{P_{atm}}$ is denoted as zero. Boyle's law, which states that, at a constant temperature, the pressure and volume of a given quantity of gas vary inversely [44], is expressed in Equation (1).

$$P_1 V_1 = P_2 V_2 \tag{1}$$

Here, in Equation (1), $\boldsymbol{P_1}$ represents the initial pressure, $\boldsymbol{V_1}$ stands for the initial volume, $\boldsymbol{P_2}$ signifies the final pressure, and $\boldsymbol{V_2}$ denotes the final volume [44]. The two primary pressures responsible for the breathing process within the lungs are intra-alveolar pressure, which exists within the alveoli, and intrapleural pressure, found within the pleural cavity. The difference between these two pressures yields the transpulmonary pressure, determining the lung's size. Lung pressures undergo fluctuations throughout the breathing cycle primarily due to the actions of the diaphragm and external intercostal muscles. It is crucial to emphasize that the lungs do not actively generate the pressure gradient during respiration. Instead, changes in lung volume and, consequently, pressure result from the tension of the pleural fluid, causing the lungs to expand outward as the chest enlarges during inspiration. During expiration, the thoracic wall recoils due to lung elasticity. Notably, inspiration is an active process, while expiration is passive, requiring no additional energy [45], [46]. During inspiration, the contraction of the diaphragm and external intercostal muscles leads to an increase in thoracic volume, subsequently lowering the pressure within the lungs, as Equation (1) suggests. Conversely, relaxation of the diaphragm and external intercostal muscles reduces the volume of the thoracic cavity and the lungs, resulting in an elevation of alveolar pressure. This pressure difference prompts the flow of air from areas of higher pressure to those

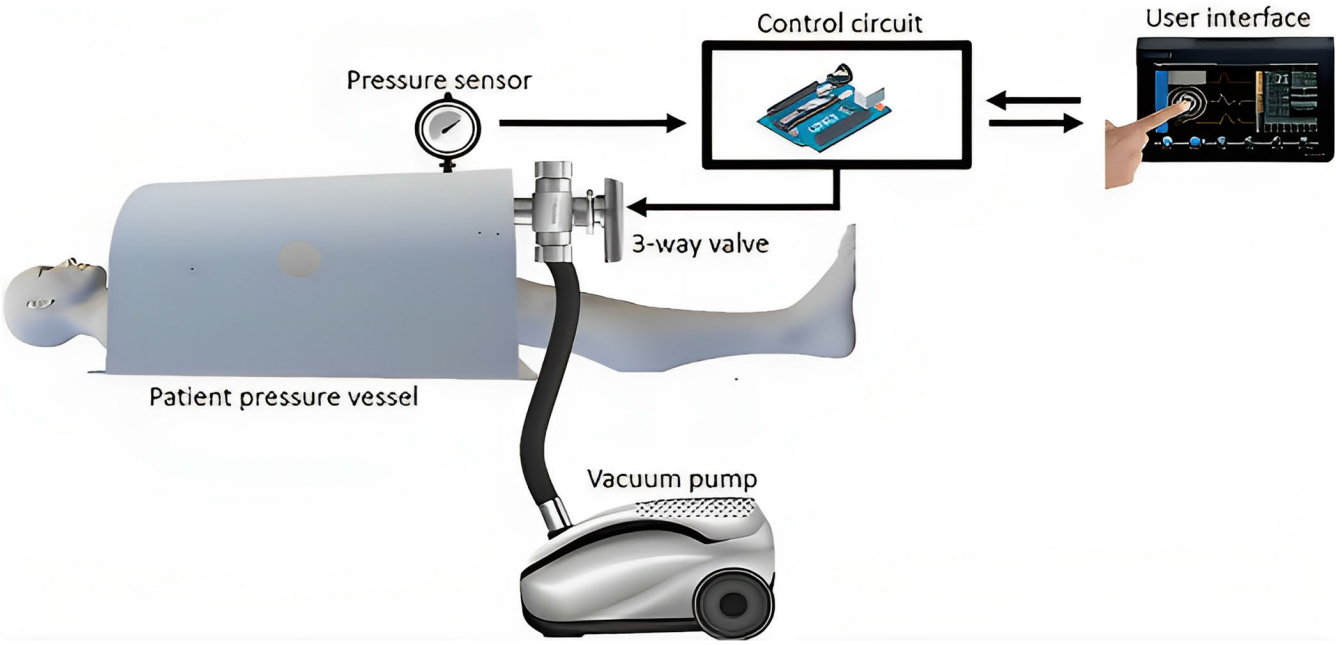

FIGURE 1. Overview of the proposed ExoventQ ventilation system: It comprises a Negative Pressure Vessel (NPV) serving as the patient pressure chamber, a 3-way Butterfly Valve, and a pump responsible for generating and regulating the vacuum within the chamber. The entire system is controlled by an Arduino-based microcontroller, which responds to user inputs through a Raspberry Pi-based User Interface (UI) and provides essential feedback.

of lower pressure, as expressed in Equation (2).

$$\mathrm{F} = \frac{P_{aw} - P_{alv}}{R} \tag{2}$$

Here, F represents the airflow, $\boldsymbol{P_{aw}}$ signifies the airway pressure, $\boldsymbol{P_{alv}}$ represents the alveolar pressure, and R corresponds to body resistance, primarily dependent on the size of the airway. Consequently, when the alveolar pressure falls below the airway pressure during pulmonary ventilation, air is drawn into the lungs. Conversely, when the alveolar pressure exceeds the airway pressure, air exits the lungs [12], [47].

III. MATERIALS AND METHODS

In this section, we will first provide a brief discussion of the overall system requirements and constraints that must be adhered to when developing the complete NPV system. In the subsequent subsections, we will delve into the detailed examination of each component of the proposed mechanical ventilator.

A. SYSTEM OVERVIEW

The understanding of pulmonary ventilation provided in Section II is essential for the design of a low-cost, safe, and portable ventilator system. As previously mentioned, the system comprises three primary components: a pressure vessel, a control system, and a pumping system, as depicted in Figure 1. The vessel needs to be comfortable, lightweight, and efficient in terms of minimizing leakage, particularly for an average adult. The pumping system must be capable of generating a vacuum inside the vessel that can reach up to 50 mbar within one second or less. This is crucial, as negative extra-thoracic pressure necessitates a vacuum pump capable of delivering a maximum vacuum of 35 mbar (approximately 35 cmH2O) with an airflow rate of 10 L/s [48]. On the other hand, the control system must provide clinicians with the ability to regulate and monitor the pressures within the vessel, control the respiratory rate (RR) within the range of 10 to 30 breaths per minute (bpm) [49], set the inspiration-to-expiration (I:E) ratio anywhere from 1:1 to 1:4, adjust the inspiration pressure (P_{insp}) between 5 to 35 mbar of vacuum, and manage the expiration pressure (P_{exp}) between 0 to 15 mbar of vacuum [50]. It is worth noting that when PPV is administered via a mask, it produces approximately 65 $\pm$ 11 dBA of noise. Consequently, the noise generated by the NPV ventilator should be equal to or lower than the noise produced by the PPV to prevent patient discomfort [49]. During practical implementation, a healthcare provider powers the device by connecting it to the mains, sets the ventilation mode, and inputs the corresponding parameters. Subsequently, the vacuum pump and the control system commence their operations. The vacuum pump creates a vacuum within the patient's chest enclosure, referred to as the pressure vessel. Simultaneously, the control system fine-tunes the vacuum inside the vessel using an adaptive feedback system to align with the parameters established by the healthcare provider. All pertinent data and the pressure wave are displayed to the healthcare provider through a user-friendly interface. The subsequent sections of this chapter will delve into the operational concept and design details of each component.

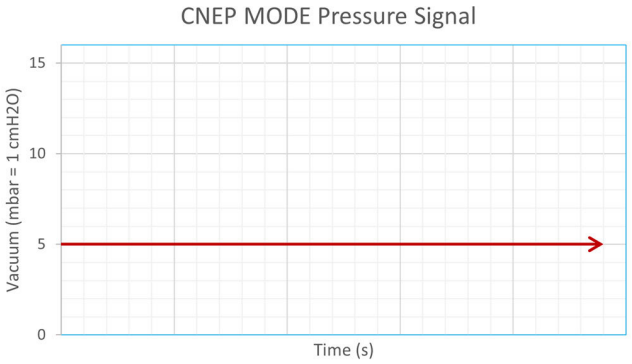

FIGURE 2. The pressure inside the patient's vessel during the CNEP mode.

B. CONCEPT OF OPERATION

Several studies have indicated that not all patients require full respiratory assistance; rather, some only need respiratory enhancement [51], [52]. This enhancement can be achieved by subjecting the patient to continuous negative extrathoracic pressure, also known as CNEP. CNEP serves to enhance lung expansion during inspiration and maintain the openness of alveoli during and after expiration, thereby preventing atelectasis [53]. The design of this system will serve as a respiratory support device rather than a ventilator. It can either support spontaneous breathing or assume complete control over the respiratory process through the following modes, respectively.

1) CONTINUOUS NEGATIVE-EXTRATHORACIC PRESSURE (CNEP)

During this mode, the vacuum pressure inside the pressure vessel remains constant, as illustrated in Figure 2. The concept is analogous to the Positive End-Expiratory Pressure (PEEP) delivered by PPVs [54]. It's important to note that vacuum pressure here is depicted as positive because the device will only be encountering sub-atmospheric pressure, making it simpler to work with the absolute value of the pressure. The CNEP level will range from 5 to 15 mbar of vacuum, allowing the patient to breathe comfortably against the negative pressure.

2) CYCLIC NEGATIVE-PRESSURE VENTILATION (CNPV)

In this mode, the pressure inside the vessel experiences a significant drop, becoming highly sub-atmospheric during inspiration and returning to zero (i.e., atmospheric) or near-zero during expiration in a cyclic pattern. This mode is equivalent to cyclic PPVs with PEEP. The most theoretical signal for achieving this function is the rectangular pulse, as illustrated in Figure 3 (a) with accompanying annotations. This signal comprises four crucial parameters: inspiration pressure (P_{insp}), expiration pressure (P_{exp}), inspiration time (T_{insp}) and expiration time (T_{exp}). T_{insp} and T_{exp} collectively determine the respiratory rate (RR), which represents the number of breathing cycles the patient undergoes in one minute. Meanwhile, the inspiration-to-expiration ratio (I:E)

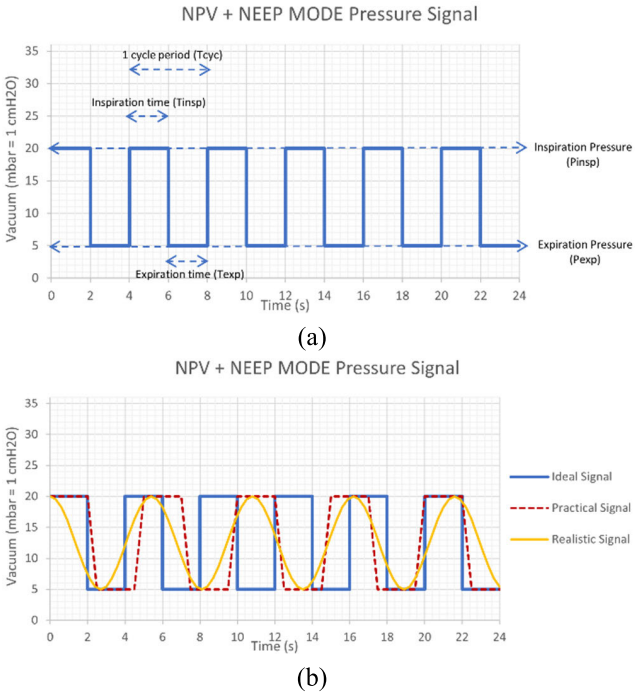

FIGURE 3. NPV mode pressure signals; (a) Ideal pressure waveform with annotations, (b) Ideal (blue) vs. Practical (red dotted) signals. The yellow line represents the pressure inside a device in a real-world scenario.

indicates the proportion of time the patient spends inhaling compared to exhaling. RR and the I:E ratio can be defined using Equations (3) and (4), respectively.

$$RR = \frac{1}{T_{cycle}} BPM = \frac{1}{T_{insp} + T_{exp}} BPM \equiv \frac{60}{T_{insp} + T_{exp}} BPS \tag{3}$$

$$I : E = \frac{T_{insp}}{T_{exp}} \tag{4}$$

Here, BPM and BPS denote beats per minute and beats per second, respectively. To calculate T_{insp} and T_{exp}, we can rearrange Equations (3) and (4) and combine them as shown in Equations (5) and (6), respectively.

$$T_{insp} = \frac{60 * I : E}{RR * (1 + I : E)} sec \tag{5}$$

$$T_{exp} = \frac{60}{RR * (1 + I : E)} sec \tag{6}$$

This system allows clinicians to set the 4 parameters within the following ranges:

- Inspiration Pressure (P_{insp}): [15 – 35] cmH2O
- Expiration Pressure (P_{exp}): [0 – 15] cmH2O
- Respiratory Ratio (RR): [10 – 30] bpm
- Inspiration to Expiration Ratio (I : E): [1:1 to 1:4]

In an improved practical approximation, the signal is expected to be trapezoidal, considering the system's response time, as illustrated by the dashed red line in Figure 3 (b). On the other hand, the Negative End-Expiratory Pressure (NEEP) [55] recorded inside a real device implemented by

our team has been depicted by the yellow waveform in Figure 3 (b).

C. PATIENT'S PRESSURE VESSEL

Throughout history, NPVs have undergone various designs, including different tanks, chambers, cuirasses, and even coats, each with its own set of advantages and disadvantages. However, the iron lung design [8] emerged as the most popular due to its geometry and material selection, simplifying the creation of negative pressure inside the vessel and providing comfort to many patients. Nevertheless, this design still had several drawbacks, primarily its weight and bulkiness, as it was constructed from iron. It occupied a significant amount of space and lacked portability [12]. The chest cuirass design [56] appeared to be a more appealing alternative, as it only enclosed the chest, allowing clinicians to care for the patient more easily and reducing restrictions on patient positioning and movement. Its lightweight and transparency, similar to the Hayek cuirasses [23], made it even more advantageous. However, these improvements were insufficient to make it efficient, mainly because the cuirass ended at the patient's upper abdomen, resulting in inadequate diaphragmatic contractions and ventilation [57]. When designing **ExoventQ**, we considered the advantages of these historical designs while addressing their drawbacks based on specific design constraints. The design criteria for the pressure vessel can be divided into two major sections: structural design and material selection, briefly explained in Sections III-C(1)-(2), respectively, based on our previously published article [58]. We also conducted ANSYS-based [59] simulations of the 3D vessel models to determine the optimal vessel architecture, as discussed in [39] with visualizations and quantitative results. Finally, in Section III-C(3), we provide details on the manufacturing process of the selected model.

1) STRUCTURE

The geometry of the vessel encompasses its shape and measurements, which are essential for selecting the appropriate material for the vessel and guiding the subsequent manufacturing process. In this study, we constrained the vessel's structure based on considerations of user-vessel interactions (involving both patients and clinicians), its tolerance to applied pressure, and compliance with clinical environments, as elaborated in [58]. The primary end user of the ventilator is the patient, and they are directly impacted by its design. Therefore, the vessel's structure must efficiently support the contractions of the respiratory muscles. Moreover, it must provide convenience, comfort, and sufficient space for the patient. For this project, we designed the vessel to accommodate an adult male with a weight range of 75-90 kg (based on the 95th percentile). Additionally, the vessel should be easily accessible to clinicians for conducting tests and monitoring patients. Vacuum pressure vessels are exposed to negative pressures, making them susceptible to a net external atmospheric pressure that acts as a compressive load and may cause the vessel to buckle, resulting in structural failure. To mitigate this risk, we conducted structural analysis on various vessel designs, utilizing 3D simulations in ANSYS [58], to determine the most robust structure for this application. Our analysis included various semi-cylindrical and rectangular prism models, ultimately concluding that a squircle-faced, semi-cylindrical structure was the most suitable choice for minimizing the potential for structural failure, as elaborated in our work in [58].

2) MATERIALS

From a mechanical perspective, three primary characteristics that help determine the appropriate choice of materials for a vessel structure are rigidity, elasticity, and toughness [60]. These characteristics are measured, respectively, by Yield strength, Young's modulus or modulus of elasticity (γ), and the area under a stress-strain curve. The developed semi-cylindrical vessel must possess sufficient strength to withstand the pressure created by the vacuum inside NPVs, necessitating careful material selection. Additionally, the chosen materials must be non-hazardous and safe for clinical environments. Transparency is also desirable to facilitate patient monitoring, and the use of lightweight materials to enhance portability [58]. For the main body of the vessel, we opted for two types of plastic: Acrylic and Polycarbonate (PC). These materials were selected due to their non-reactive nature, poor conductivity, strength, and durability. Reduced reactivity with other materials and poor heat and electrical conductivity ensure safety in a clinical environment. On the contrary, maintaining portability while being durable is challenging. Acrylic materials, in general, possess a tensile or Young's modulus (γ) of 3.2 Gigapascal (GPa) against 2.6 GPa of Polycarbonates. Moreover, the ultimate tensile strength of the Acrylic materials (70 Megapascal or MPa) is also higher than the Polycarbonate materials (52-62 MPa) [61]. Regardless, Polycarbonate was preferred over Acrylic because Acrylic devices are more susceptible to cracking during drilling or when subjected to impacts [58], challenging both the durability and safety criteria.

Conversely, the selection of materials for the seals is critical, as they determine the system's leakage. Seals must be highly elastic and flexible while remaining biocompatible to prevent skin issues for the patient. We compared neoprene (or polychloroprene, one type of synthetic rubber) and latex (or natural rubber) and found that neoprene (0.00614 GPa) is much more flexible than latex (0.1 GPa) [61]. Although latex can withstand more tension, it may cause allergies in some individuals due to the presence of latex protein [62]. As a result, neoprene was chosen.

3) MANUFACTURING THE FIRST PROTOTYPE

Once the structure of the vessel had been finalized through simulation and materials had been selected based on datasheets, we commenced the initial prototype

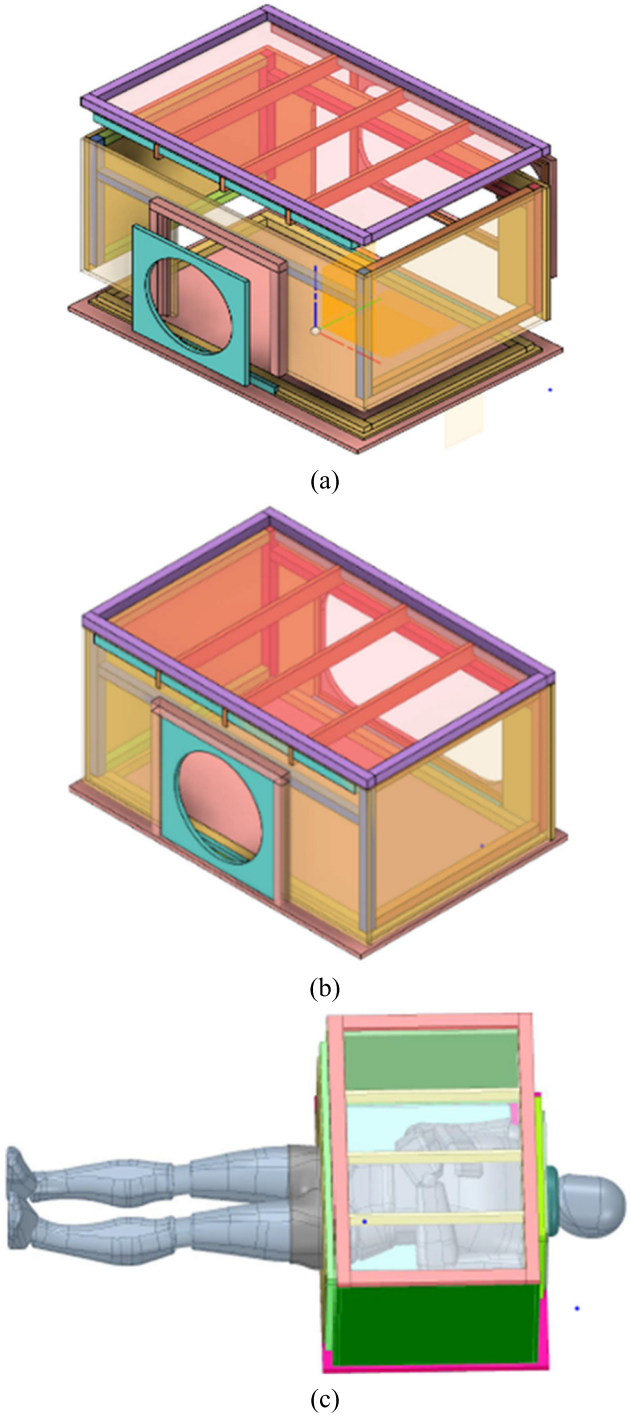

FIGURE 4. 3D design of the wooden prismatic vessel for operation testing: (a) exploded view, (b) assembled view, (c) subject's position inside the vessel.

manufacturing process. For this purpose, we opted for a wooden prismatic vessel as our test prototype. This choice was made based on several criteria, including material availability, affordability, workshop accessibility, ease of modification (e.g., drilling and cutting), ease of manufacturing, and the convenience of installing components inside the vessel for testing purposes. To begin, we created a model

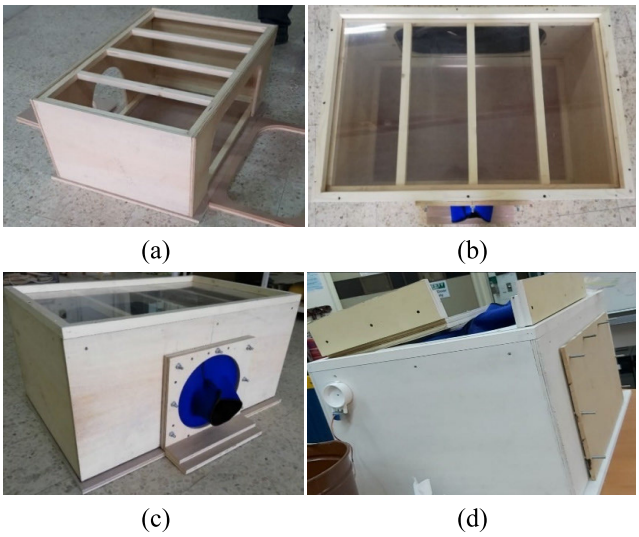

FIGURE 5. Wooden prismatic testing vessel manufacturing process, gradually developed from stage (a)-(d).

of the vessel using Fusion360, specifying dimensions such as length (L) = 0.9 m, width (W) = 0.64 m, and height (h) = 0.415 m, with a vessel thickness of 12 mm. To prevent bending and minimize deformation, we incorporated support battens and a 25 mm thick girder, as illustrated in Figure 4 (a) and (b).

The structure contains two holes, one for the neck and the other for the torso. Neoprene seals [63] are attached to separate boards with holes of the same radius as the neck and torso holes. As shown in Figure 4 (c), the test subject wears the seals and lays them down on the baseplate. Then the removable upper body of the vessel is placed over them, and the boards are tightly attached to the main body using screws. It is important to note that in case the materials needed to build the polycarbonate semi-cylindrical vessel are unavailable, this wooden prismatic vessel can serve the purpose. However, it may not fully meet all the device constraints. Nonetheless, it can be used as a life-saving measure once the device has been proven to function properly. The primary materials used to construct the wooden prototype are 12 mm plywood, 25 mm white solid wood, flexi-glass, and rubber seals. Components such as wood glue, nails, 5 cm screws, nuts, and bolts of various sizes were required for assembly. The manufacturing of the wooden prismatic pressure vessel went through several phases, as shown in Figure 5.

The manufacturing process was divided into five phases: material cutting, main body assembly, neck-seal and torso-seal assembly, structural finishing, and finally, preparing the vessel for testing. In the first phase, plywood, white solid wood, and flexible glass were cut according to the specified dimensions. This phase also involved Computer Numerical Control (CNC) laser cutting of neck and torso panels to create the required holes. In the second stage, the neck and torso panels, along with their support batons, were attached to the frame of the top panel using wood glue, nails, and screws.

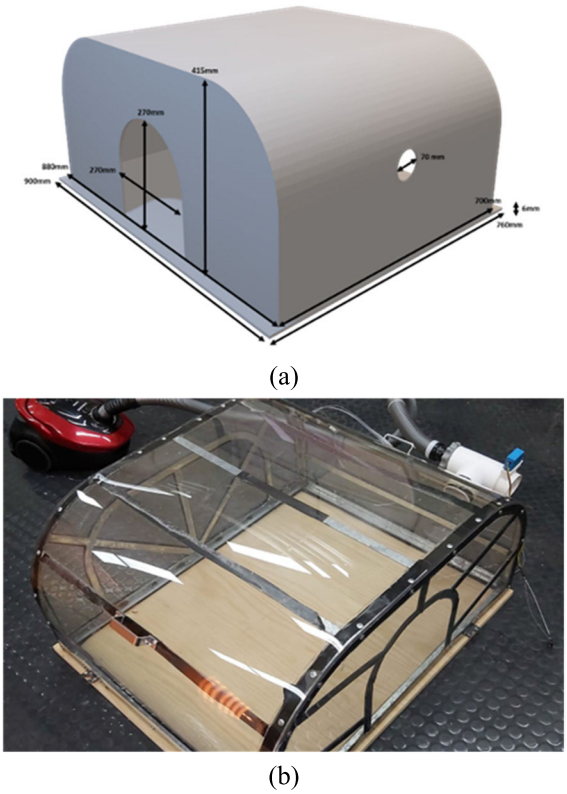

(a)

(b)

FIGURE 6. (a) 3D model of the polycarbonate (PC) squircle-faced vessel [58], (b) implemented PC vessel.

Baseplate batons were assembled with rubber seal strips surrounding them. Wooden girders were then assembled to the top panel frame to hold the flexi-glass sheet. In the following stage, the neck and torso rubber seals were affixed to removable wooden boards that could be attached and detached from the main neck panel via bolts and nuts. The next phase focused on improving the vessel's appearance by painting it white from the outside. The final phase involved preparing the vessel for operational testing. This included drilling holes for the suction tube and the control valve, attaching the tube and the valve, and sealing the holes with solid boards to ensure the device's functionality under extreme conditions, such as minimal leakage, before testing it on subjects using the neck and torso seals.

4) DEVELOPING THE POLYCARBONATE VESSEL

After testing the operation with the wooden prototype, it was time to implement the Polycarbonate (PC) vessel. However, instead of creating a typical semi-cylindrical vessel, we structured a squircle-faced vessel based on the simulation results discussed in [58], as illustrated in Figure 6. We opted for this design because a perfect semi-cylindrical vessel would cause a tilt in the suction tube and the valve when assembled, potentially altering the airflow. Additionally, a squircle-faced vessel maintains the volume of the wooden vessel, eliminating the possibility of pressure changes due to volume alterations, as suggested by Equation (1). The vessel was initially modeled in Fusion360 with dimensions as follows: length (L) = 0.9m, width (W) = 0.76m, and height (h) = 0.415m. The thickness of the vessel was set at 3 mm. Although the vessel would not experience permanent deformations, as discussed in Section III-C(1), it would undergo deformations when pressure was applied. Therefore, a steel support structure was created to minimize these deformations.

The materials used for the earlier prototype differ from those used for the final PC vessel, which were carefully selected through qualitative and quantitative analysis, as discussed in Section III-C2). The materials used for the main body of the vessel include 3 mm transparent polycarbonate, 2 mm galvanized steel, 18 mm plywood, 3 mm transparent acrylic, and rubber seal. Additionally, the tools employed for assembly consist of metal self-drilling screws, normal screws, wing nuts, double-face tape, and clear silicone. Similar to the wooden prototype, the manufacturing of the PC vessel was divided into five stages: material preparation, building the steel support structure, main body assembly, neck seal and torso seal assembly, and vessel preparation. During the material preparation stage, PC sheets were cut and bent for the main body of the vessel, a wooden board was cut for the baseplate, acrylic sheets were cut for the seal boards, and some steel sheets were bent for the support structure. In the second phase, the steel support structure was constructed by welding steel sheets into the shape of the vessel. In the third phase, the PC sheets were assembled onto the steel structure using screws and sealed with double-face tape and clear silicone. In the fourth phase, seals were attached to the acrylic boards. Finally, necessary holes were created for the bypass valve and the wiring of the sensors attached to the vessel from the inside.

D. PUMPING SYSTEM

Throughout history, various pumping and control techniques have been employed to generate and regulate the vacuum within the patient's vessel. In contrast to the widely known Emerson iron lung [9], which featured bellows covering almost the entire body [12], **ExoventQ** has been designed to allow full access to the lower half of the patient's body. Therefore, the patient's body will not be entirely enclosed by the chamber. Since bellows cannot be utilized in **ExoventQ** to create a vacuum inside the vessel, we have developed an alternative pumping solution. Section III-D(1) will provide insights into the pumping system of **ExoventQ**. Additionally, in Section III-D(2), we will delve into the significance of controlled leakage within the system and present our solution.

1) PUMPING SYSTEM: AIR SUCTION

A vacuum pumping system can be achieved through various methods. One of the simplest and readily available systems is the motor-blower system [64]. When the motor is connected to the mains and activated, it rotates the shaft, which in turn rotates the impeller. Air is drawn into the impeller's eye,

TABLE 1. Specifications comparison among different motor types.

Criterion	Universal DC	Induction	Brushless DC
Power	Low	High	High
Noise	High	Low	Low
Control	Simple and inexpensive	Complex and expensive	Complex and expensive
Size	Acceptable	Bulky	Small
Cost	Low	High	Moderate
Maintenance	Periodic	Less	Less
Longevity	Shorter	Longer	Longer
Efficiency	Moderate	High	High
Availability	From off-the-shelf vacuum cleaners	Off-the-shelf	Off-the-shelf

where its velocity increases as it moves along the blades. Eventually, due to centrifugal force, the air is expelled from the blades at the outlet, resulting in a decrease in velocity. This movement of air from the eye to the blades generates low pressure at the eye, causing air to rush into the motor blower and out of the vessel, thus creating a negative pressure. Conversely, the lower velocity of air at the outlet leads to the formation of higher pressure, which expels the air to the exterior. Consequently, we need both a motor and a blower for the pumping system. In this study, we explored three common types of motors: universal DC motors, induction motors, and brushless DC motors. We evaluated these motors based on criteria such as power, noise, control, size, cost, maintenance, longevity, efficiency, and availability, as detailed in Table 1.

According to Table 1, Universal DC motors are typically smaller in size and generate less power, which makes them cost-effective [65]. In contrast, Induction motors are the bulkiest, strongest and the most expensive, while Brushless DC motors fall somewhere in between, being moderate in most aspects [66]. However, the specific features of the Universal DC motor, namely its small size, low cost, simple control, and widespread availability, align with the desired characteristics of the designed MV prototype discussed beforehand. Therefore, the Universal DC motor was chosen.

For motor-blower systems, apart from motors, the other crucial component, known interchangeably as fans, is a blower [64]. These mechanical devices facilitate airflow. For this study, we examined three types of blowers: positive displacement blowers, centrifugal air blowers, and regenerative blowers [67]. In theory, the most dependable system for **ExoventQ** would involve an induction motor powering the blower system. However, it is unlikely that an induction motor will precisely match the vacuum impeller's requirements. On the contrary, an off-the-shelf vacuum blower is the most suitable option for this project, given its accessibility and cost-effectiveness, commonly found in everyday items such as vacuum cleaners, leaf blowers, spa bath blowers, and industrial vacuum blowers. Despite the advantages of other motor and blower types, we opted for the universal DC motor in conjunction with a centrifugal air blower from a vacuum cleaner for the vessel's pumping system due to its widespread availability. The Samsung VC2032510 200W vacuum cleaner [68] utilized in this project can achieve a maximum vacuum of 15000 Pa (approximately 150 cmH2O) and deliver around 13 L/s of airflow. Additionally, it is compact and offers multiple speed control levels.

TABLE 2. Comparison among the studied valve types.

Criterion	Gate Valve	Butterfly Valve	Piston Valve
Cost	Moderate	Low	High
Availability	Low	High	Low
Isolation	High	Moderate	High
Reliability	High	Moderate	High
Safety	Moderate	High	High

2) CONTROLLED LEAKAGE

The pumping system, by itself, cannot meet the requirements of this device. Assuming an ideal completely sealed vessel with zero leakage, the continuous suction process would lead to an increasing vacuum inside the vessel until all the air particles are drawn in. In reality, this means that even if the motor speed remains fixed (i.e., the air outflow remains constant), the pressure inside the vessel will continue to decrease and will not stabilize. Therefore, to maintain a steady pressure, there must be an inflow of air to balance the excess vacuum, which can be achieved through the use of valves. Valves can be broadly categorized as fully open or closed valves and partially open valves, each with several subtypes [69]. Among the most common partially open valves are gate valves, butterfly valves, and piston valves [70]. Table 2. provides a comparison of these valves in terms of cost, availability, isolation, reliability, and safety.

The most suitable valve for this project was found to be the butterfly valve as it has a very low cost, can be easily supplied at a high production rate, and is relatively safe for operation at low-pressure levels, which, for this project, can reach up to 50 mbar of vacuum.

E. CONTROL SYSTEM

As discussed in Section III-C, the main parameters to be controlled in the system are the pressure inside the vessel, which varies within a certain range, and the amount of time each pressure is held, controlled based on a specified ratio (I:E) and RR. There are two major types of control systems: open-loop and closed-loop [71]. An open-loop control system is equivalent to implementing a blind control system, which issues commands to either the motor or the valve but does not incorporate any feedback mechanism. Therefore, a closed-loop control system has been deemed more suitable for this project. In a closed-loop system, feedback will be provided by a differential pressure sensor. However, there won't be a direct mathematical relationship between the speed of the blower or the angle of the valve and the pressure inside

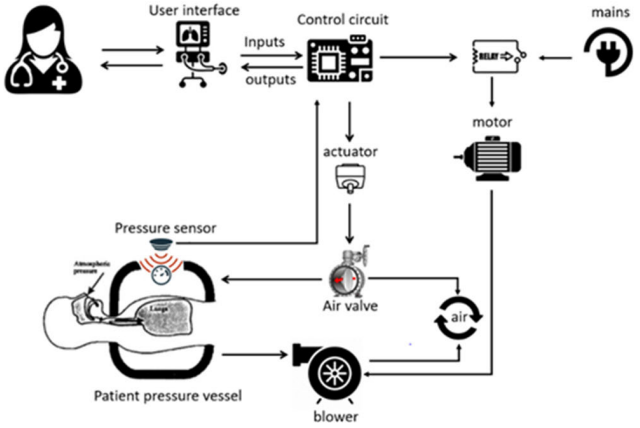

FIGURE 7. Complete layout of the control system.

the vessel, which will be further explained in this chapter. Section III-E(1) will discuss the sensors and indicators used in this project to implement a closed-loop system and enable device monitoring, while Section III-E(2) will delve into the possible control system components, the selected components, and the system's implementation. The overall layout of the control system is provided in Figure 7.

1) SENSOR SELECTION AND CHARACTERIZATION

In this study, we acquire and monitor two broad types of physical quantities inside the vessel: pressure caused by the vacuum and temperature, to ensure that the patient does not experience a ''tank shock'' [72]. For each type, we select suitable sensing modules and characterize them against standard units before conducting tests.

a: PRESSURE

We placed a digital pressure sensor inside the vessel to measure the vacuum pressure, which required verification against a reference. In the laboratory, we constructed a 2-meter-long Manometer [73] to serve as the ground truth. A Manometer is a device used to measure static pressure. It consists of a U-shaped tube filled with a dense and incompressible fluid. To measure the pressure inside a chamber, one end of the U-shaped tube is connected to the patient's pressure vessel, while the other end is exposed to the atmosphere. When the pressure inside the chamber decreases, the liquid level rises on the side connected to the chamber. When there is no pressure difference inside the vessel (i.e., atmospheric pressure), the fluid level equalizes on both sides of the U-shaped tube, a state known as ''Hydrostatic Equilibrium'' [74]. With this increase in height, the pressure of the fluid inside the chamber can be measured using Equation (7).

$$P = \rho g(\Delta h) \tag{7}$$

In this equation, P represents the pressure of the system, ρ stands for the fluid density (which is 1000 $\boldsymbol{kgm^{-3}}$ for water [75]), g is the acceleration due to gravity (average g on the earth's surface is 9.81 $\boldsymbol{ms^{-2}}$ [76] which has been considered for this study), and Δh denotes the change in fluid level. The handmade Manometer serves as a valuable ground truth to verify the proper calibration of the digital sensor. To cover a wide range of pressure, we chose a Manometer with a length of two meters. This method incurs minimal error and does not necessitate further calibration. The process has been visualized in **Supplementary Figure S1**. The selected digital sensor requires characterization of the applied voltage to convert the analog temperature readings into a digital range determined by the device's analog-to-digital converter (ADC). Digital data can be stored, processed, transferred, or employed for controlling other parameters. However, to use this data effectively for display or control purposes, it is essential to establish the relationship (slope and intercept) between the analog (temperature) and the converted digital units. Therefore, we conducted pressure vs. voltage characterization.

TABLE 3. Temperature sensor selection criteria.

Criterion	DHT22	DHT11	LM35
Cost (USD)	9.95	5.00	2.5
Calibration	Not Required	Not Required	Required
Temperature Accuracy	± 0.5 degrees	± 2 degrees	± 0.5 degrees
Humidity Accuracy	± 2-5%	± 5%	± 0.75%
Measuring Range	-40°C to +125°C	0°C to 50°C	Depends on calibration
Operating Voltage	3 to 5	3 to 5	4 to 30
Operating Current	2.5 mA	2.5 mA	114 µA

b: TEMPERATURE

To prevent the patient from experiencing a ''tank shock'' [72], it is crucial to monitor the temperature inside the pressure vessel, as previously discussed. We primarily had three options to consider: DHT22 [77], DHT11 [78], and LM35 [79]. We analyzed all three module types and determined that DHT22 was the most suitable choice based on the evaluation criteria outlined in Table 3 and their respective datasheets.

The selection of the DHT22 sensor for this study was based on its ease of installation and programming, as well as its high level of accuracy when compared to the other available modules. The DHT22 is an enhanced version of the DHT11 and, while being more expensive, offers the latest features and specifications, resulting in improved accuracy and precision. Moreover, it boasts a wider operating range for temperature and humidity, with the added benefit of not requiring external calibration (as it includes calibration software). However, to ensure its accuracy, the DHT22 module underwent testing alongside a well-established operating device (a digital thermometer) known for its precise temperature measurements, as depicted in **Supplementary Figure S2**. The temperature accuracy difference was found to be approximately ±0.5 degrees across the operating range of the DHT22.

TABLE 4. Comparison between motor and valve control.

Criterion	Motor Control	Valve Control
Complexity	High	Low
Reliability	More	Relatively Less
Maintenance	High-cost periodic maintenance	Low-cost periodic maintenance
Noise	More	Less

TABLE 5. Comparison of actuators.

Criterion	Servo	Stepper	DC
Cost	Low	Moderate	High
Availability	High	High	High
Torque	Moderate	Low	Moderate
Controlled motion	High	Moderate	Moderate
Response speed	High	Low	Moderate
Angle precision	Moderate	High	Moderate
Control complexity	Moderate	Low	High

2) ACTUATOR CONTROL MECHANISMS

To control the two parameters, pressure, and temperature, mentioned at the beginning of this section, two primary approaches can be followed. The first approach involves controlling the air outflow, which can be achieved by regulating the motor speed and, consequently, the blower speed. Alternatively, this approach can also be implemented using a bypass valve that allows the pump to either draw air from the vessel or the environment, depending on the desired pressure inside the vessel. The second approach focuses on controlling the air inflow, which can be managed using a leakage valve that governs the volume of air entering the vessel. Table 4 provides a comparison between controlling the motor and the valve [80], to assist in determining the most suitable approach for this study. Valves can be controlled either manually or automatically with the use of an actuator. A manually controlled valve may be practical in CNEP mode, where the pressure remains constant and does not require frequent adjustments. However, manual valve control becomes entirely impractical during NPV mode, considering that the entire breathing cycle can last a maximum of 6 seconds when the respiratory rate is set to 10 bpm. This necessitates the use of an actuator to control the valve. The system overview, as illustrated in Figure 7, provides details of the control system implemented in this project.

Table 4 indicates that valve control offers more advantages compared to motor control. This choice allows for flexibility in selecting between the two approaches for valve control, either regulating air inflow or outflow. Controlling air inflow would necessitate creating two holes in the vessel, one for the tube connected to the vacuum pump and another for the valve. However, this approach may present challenges because additional holes in the vessel can lead to more uncontrolled leakage, particularly considering the potential high uncontrolled leakage from the neck and torso seals. On the other hand, controlling air outflow through a valve would require only one hole in the vessel. A 3-way pipe would connect to the vessel, with one side linked to the vacuum tube and the other to the valve. Consequently, regulating air outflow via a valve appears to be the most suitable control approach for this project, based on our assessment. Various types of actuators can be used to control a valve's performance, including servo motors, stepper motors, and DC motors. These actuators can be linked to a driver board and controlled through a microcontroller. To ensure optimal performance, specific selection criteria have been established, encompassing factors like cost, availability, torque, controlled motion rate, response speed, angle precision, and control complexity, as outlined in Table 5 [81], [82], [83].

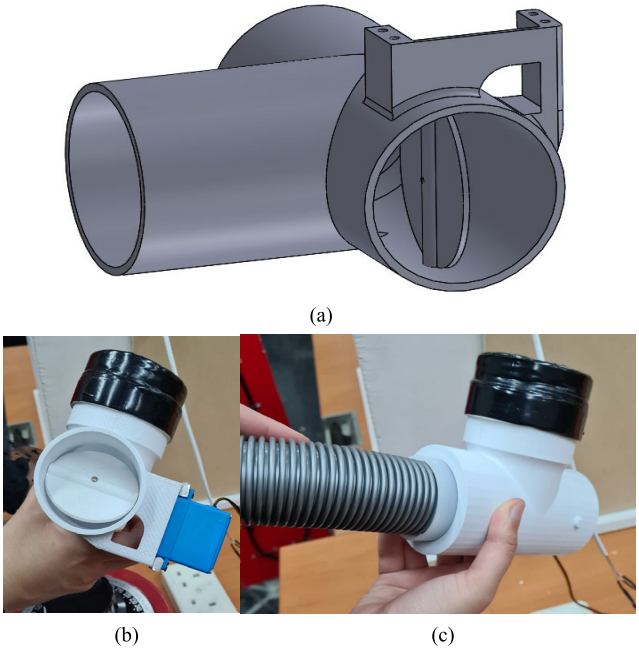

FIGURE 8. 3-way Butterfly valve: (a) 3D model designed in a Computer-Aided Design (CAD) software; 3D printed (b) top view, (c) side view.

Precisely controlling the vacuum pressure within the vessel relies on two primary parameters: high-angle precision and sufficient torque to withstand the pressure acting against the valve's movement. Conversely, when it comes to controlling RR and I:E ratio, response time assumes critical importance. To maintain cost-effectiveness and simplicity, DC motors were initially ruled out as an option. Stepper motors offer precision and relatively fast performance. However, they cannot provide information about the angle at which they are positioned, as they do not incorporate a feedback system. This limitation poses an issue since knowing the valve's angle is essential for using it as an input within the system. On the other hand, servo motors exhibit movement relative to their original position (i.e., 0° angle), allowing the system to accurately track the valve's angle. The servo motor selected for this project is the HS-646WP Waterproof Servo Motor [84]. This actuator possesses substantial power thanks to its metal gears, enabling it to move the valve with ease even against the suction force, thanks to its high torque.

FIGURE 9. Graphical User Interface (GUI) design: (a) Main panel annotated, (b) mode selection (current *mode is NPV or cyclic); (c) safety control panel, (d) UI showing severe alarm test condition.

It's important to note that not only does the angle at which the valve is opened affect the airflow rate, but also the size of the valve. After experimenting with various sizes of butterfly valves, a 3D model of a 2-way butterfly valve from the Exovent team [85] was adapted to create a 3-way butterfly valve, as depicted in Figure 8 (a). One side of the designed valve accommodates the valve's flap, while the vacuum tube is attached to the other side. The valve is affixed to the vessel through its center. The flap remains fixed within the body using a spindle, which connects to the actuator's shaft. The valve was 3D-printed using Polylactic Acid (PLA) [86] due to its cost-effectiveness and practicality, as shown in Figure 8 (b).

3) CONTROL ALGORITHMS AND CODING

To control the actuator, and consequently, the valve, we utilized an Arduino Uno microcontroller [87], known for its cost-effectiveness, wide availability, and ease of programming in the Arduino integrated development environment (IDE) [88]. This environment offers various built-in libraries, including the servo motor library, and enjoys robust support from a vast online community. The code comprises multiple functions and operates within a continuous loop upon device startup. One of these functions was designed to collect pressure sensor data in terms of voltage and convert it into cmH2O values, using a characterization equation derived from plotted data (slope and intercept). Another function calculates the inspiration (T_{insp}) and expiration (T_{exp}) times. An important algorithm dynamically controls the pressure inside the vessel based on the angle or position of the valve, which is controlled by a servo motor. This function senses the pressure at the specified position and adjusts it if it deviates by more than ± 0.5 cmH2O from the set pressure (P_{set}). Notably, at 0°, the valve is fully open, and at 90°, it is fully closed. Therefore,

if the sensed pressure falls below the set pressure (P_{set}, expiration, or inspiration), the angle or position is incremented to reduce the air inflow, thus increasing the pressure within the vessel. The reverse action is taken if the sensed pressure exceeds the set pressure. However, the degree to which the valve moves at any given time depends on the error (i.e., the difference between the set pressure and the sensed pressure). If the error is less than 10 cmH2O, the angle is adjusted incrementally by 1. If it exceeds 10 cmH2O, the angle is adjusted incrementally by 10. Another function moves the motor to the expiration position, initially set at angle zero, and waits for T_{exp} seconds, and then adjusts the position using the servo motor control function if the error exceeds |0.5| cmH2O. Subsequently, it moves to the inspiration position, initially set at angle zero, waits for Tinsp seconds to adjust the position, and resets the overflow counter. A flowchart illustrating the control system's logic is provided in **Supplementary Figure S3**. Experimental results and visualizations of the control system are presented in the Results and Discussions section (Section IV).

F. USER INTERFACE

The User Interface (UI) serves as the primary point of interaction between clinicians and the system. A user-friendly and robust interface is essential, as it empowers clinicians to effortlessly monitor and control the system's behavior. In this context, the UI has been implemented on a 7-inch touchscreen, which is powered by a Raspberry Pi (RPI), a single-board computer [89]. This interface displays real-time data on pressure, temperature, and flow within the vessel. Moreover, it provides clinicians with the flexibility to choose between two modes: NPV (cyclic) and CNEP. When the CNEP mode is selected, clinicians can set a static pressure to be maintained within the vessel. In contrast, the cyclic mode allows for the configuration of maximum and minimum negative pressure values for inspiration and expiration phases.

To set up the RPI module, one needs to begin by downloading the Raspbian OS [90] onto the memory card that is inserted into the RPI. Afterward, the RPI is connected to the touchscreen using a ribbon wire, and a wired keyboard and mouse can be attached to the RPI, which simplifies the process of writing the required code to be used for communication. The UI design, complete with annotations, is presented in in Figure 9 (a). This interface features buttons on the right side and knobs at the bottom, which clinicians can utilize for adjustments. Meanwhile, the left panel displays information gathered from the sensors connected to the microcontroller, and the central area showcases the pressure waveform. Beginning with the buttons on the right, the first button flashes to indicate an alarm when the pressure deviates from the clinician's preset values, as illustrated in in Figure 9 (c). The activation of the alarm is contingent upon parameters configured by the clinician within the ''alarm limits'' button. This setting allows them to specify the alarm frequency and define moderate and severe levels of pressure variation, as depicted in in Figure 9 (d).

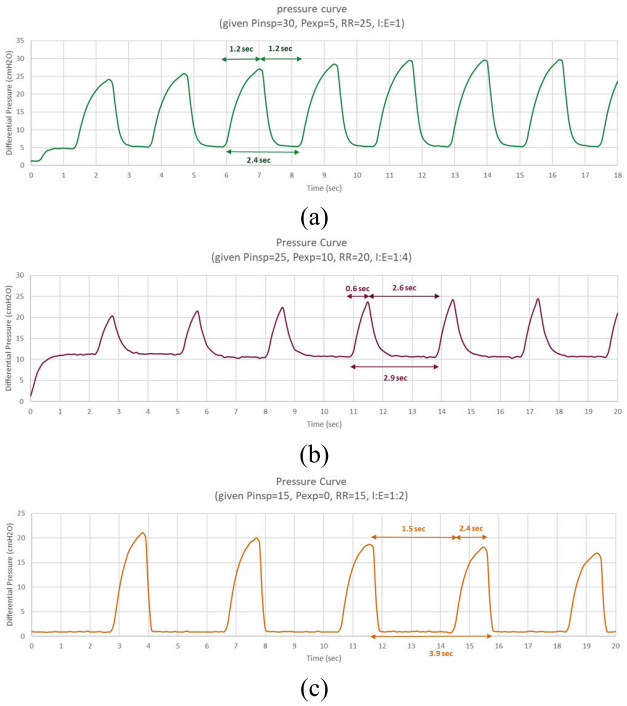

FIGURE 10. Control system test results for the NPV mode - cyclic pressure curves for various input and output parameter values.

The user initiates the system by pressing the ''Start'' button, at which point the valve begins adjusting to meet the preset inspiration and expiration pressure levels, I:E ratio, and RR. Upon clicking the button again, it transforms into a stop button, which halts the valve and motor movement. The ''Mode'' button enables users to switch between the two available modes: cyclic and CNEP. As depicted in in Figure 9 (b), the default mode is cyclic. When the CNEP mode is selected, all knobs except the one for expiration pressure are disabled, and only the expiration pressure and temperature are displayed on the left side of the screen. The knobs located at the bottom of the screen allow users to set inspiration and expiration pressures, I:E ratio, and RR from a predefined range suitable for the patient. The inspiration pressure ranges from 15 to 35 cmH2O, while the expiration pressure ranges from 0 to 15 cmH2O. Additionally, the I:E ratio is limited to preset values of 1:1, 1:2, 1:3, and 1:4. Finally, the RR can be adjusted within the range of 10 to 30 bpm. The left side of the screen displays data received from the microcontroller, which includes inspiration pressure, expiration pressure, I:E ratio, RR, and temperature. Pressure data is collected using a digital pressure sensor, while temperature data is obtained via a DHT22 temperature sensor mentioned earlier. The pressure values over time are presented in the middle of the screen as a waveform. The UI was programmed using Hypertext Markup Language (HTML) [91], Cascading Style Sheets (CSS) [92], and JavaScript (JS) [93], which are programming languages used for web page development. The UI is hosted by ''localhost,'' a virtual web server used on the local computer, i.e., the RPI module.

1) DATA TRANSFER

Communication between the microcontroller (Arduino Uno) and the RPI is achieved through serial communication, wherein data is transmitted one bit at a time sequentially, employing the Universal Asynchronous Reception and Transmission (UART) protocol [94]. UART is chosen for its simplicity and multi-master protocol characteristics, allowing multiple devices to initiate communication. The Arduino and RPI can be connected for serial communication using either Universal Serial Bus (USB) or General-Purpose Input/Output (GPIO) pins. Using USB is simpler, as GPIO pins would necessitate a voltage level shifter due to the RPI operating at 3.3V, unlike the Arduino, which operates at 5V. Clinicians input essential information via the touchscreen as required for the device's operation, as outlined in the UI. Communication between the Arduino and RPI is programmed using Python on the RPI, with data transmitted in bytes. Once communication is established, the Python script retrieves data such as start/stop commands, mode selection, inspiration pressure, expiration pressure, I:E ratio, and RR from the buttons or knobs in the UI. This data is then sent via serial communication to the Arduino, enclosed within a frame marked by a start marker '<', an end marker '>', and commas to separate different parameters. The use of start and end markers is crucial for both the Arduino and RPI to identify the beginning and end of a frame, while the commas facilitate the distinction of various values in a specific order. The RPI transmits the same frame multiple times to the Arduino until it successfully receives the values. Following this, the RPI ceases data transmission until a new alteration is made in the UI and the Arduino requires an update. In response, the Arduino provides data to be displayed in the UI, acquired from the sensors, and appends a frame number. This frame number increments when new, non-repeated data is received from the RPI. The RPI verifies the successful reception of the frame by checking whether the frame number has been incremented.

On the Arduino side, the code operates by receiving data and storing it in a buffer when the start marker is detected, and the buffer is filled once the end marker is received. Here, the buffer is compared to the previous buffer to identify duplicates, and if it's not a duplicate, the frame number is incremented, and the data is parsed. To initiate the system, it checks for the ''start'' command to become true. Based on this condition, it calculates the duration for inspiration and expiration using the received I:E and RR values. It then moves the valve accordingly to reach the designated inspiration and expiration pressure, depending on the selected mode. These conditions also activate a solid-state relay to close, which starts the motor and increases the pressure inside the vessel. The output from the Arduino includes data collected from sensors, such as inspiration and expiration pressures and temperature, along with the time information derived from counters responsible for valve control. The frame sent from the Arduino to the RPI encompasses the frame number, the 'start' data received from the RPI, inspiration, and expiration pressures, pressure data for the curve, inspiration and expiration times obtained from the counter, and temperature. These data elements are enclosed within start and end markers and separated by commas. The RPI receives the frame, decodes it, and divides the frame into variables, which are then transmitted for display on the UI. The data transfer process is illustrated in **Supplementary Figure S4**. The results of the Arduino IDE and the RPI-based UI are presented in the results and discussion section (Section IV).

G. SAFETY FEATURES

ExoventQ incorporates two layers of safety protocols: alarms (both audio and visual) and a vacuum relief system designed for emergencies. Both subsystems are elaborated upon below.

1) ALARMS

Two types of alarms have been investigated in this study: audio and visual alarms. In this system, a moderate alarm is implemented by flashing the alarm button in orange to indicate a moderate deviation from the pressure set by the clinicians. On the other hand, a severe deviation in pressure level from the set value triggers a buzzer to sound, changes the alarm button's color to red, and displays text to the left of the button, providing details about the fault. The responses of the alarm systems on the RPI-based GUI are discussed in Section IV.

2) VACUUM RELIEF SYSTEM

Since a dangerous pressure increase can occur within seconds, an extra safety feature has been incorporated into the system. This feature automatically alleviates pressure in the event of a system failure. In cases of system failure, immediate vacuum relief is essential should pressure spike within the vessel. A solid-state relay [95] has been integrated to respond when the pressure inside the vessel reaches a specific threshold. When triggered, it will disconnect the power supply to the motor, thereby eliminating negative pressure around the patient.

IV. RESULTS AND DISCUSSION

In this section, we present the various experimental outcomes of our proposed **ExoventQ**mechanical ventilator prototype for the ICU patients. We also perform a comparative analysis with the state-of-the-art ventilator systems developed during COVID-19.

A. CONTROL SYSTEM TEST RESULTS

We test **ExoventQ** control system for both NPV (cyclic) and CNEP modes by recording the data stream directly from the Arduino serial monitor [96]. In Figure 10, we present the cyclic pressure curves from the NPV mode, which include various P_{insp}, P_{exp}, RR, and I:E values recorded over 20 seconds. We change these parameters externally using the control panel to check and visualize the device response.

On the other hand, Figure 11 displays the test results from the CNEP mode for various P_{exp} values measured in cmH2O

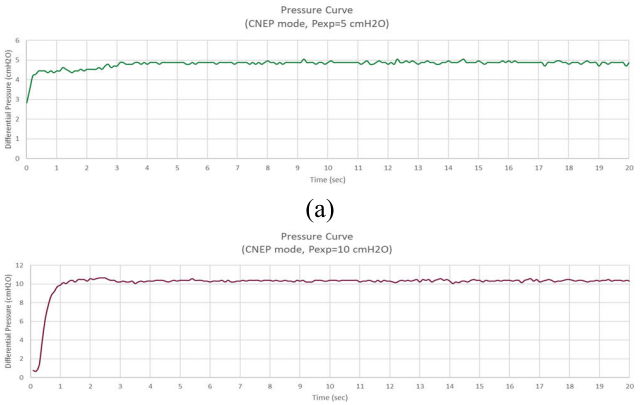

FIGURE 11. Control system test results for the CNEP mode - constant pressure curves at various P_{exp} levels.

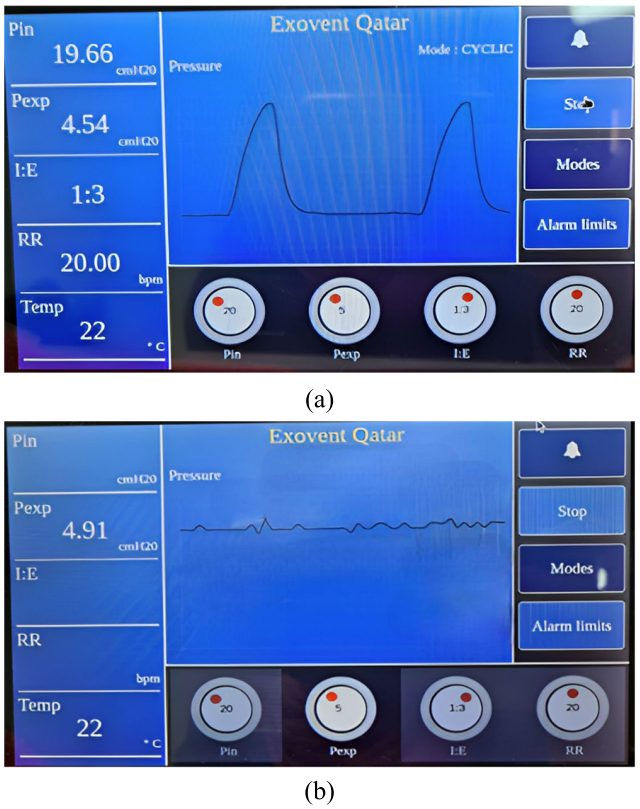

FIGURE 12. Full system testing in the (a) NPV (cyclic) mode, and the (b) CNEP mode.

over 20 seconds. An ideal plot representing the CNEP mode, as shown in Figure 2, is a constant, straight line. However, in a practical scenario, the device requires some time to build up pressure and reach the set target to satisfy the CNEP mode. In Figure 10 and Figure 11, the plots do not exactly start from zero pressure at the zeroth second, as we began recording the data after a few seconds of the device's activation. Nevertheless, the primary objective was to demonstrate a practical scenario.

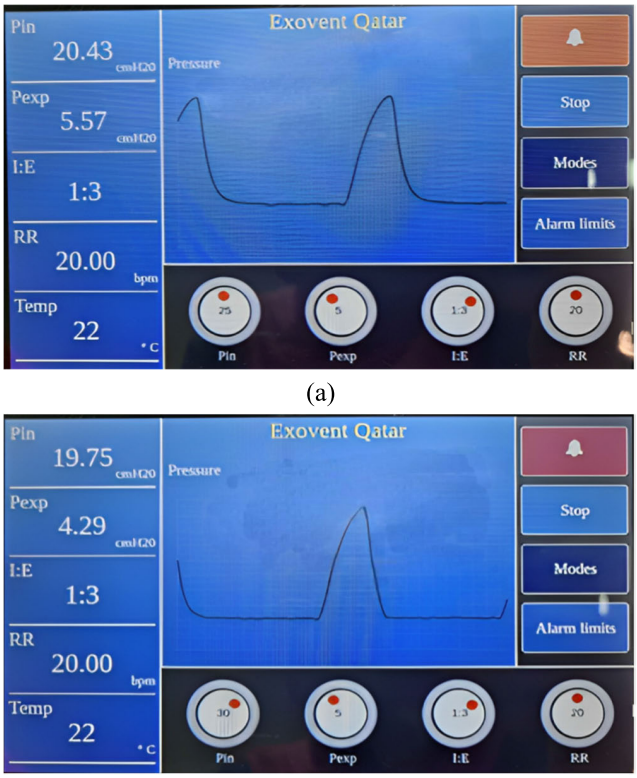

FIGURE 13. Safety alarm testing for (a) moderate, and (b) severe test scenarios.

B. FULL SYSTEM TEST OUTCOMES FROM THE UI

To assess the complete system, we conducted field tests to ensure proper data communication in both directions, i.e., between the Arduino IDE and RPI. Clinicians input the data (P_{insp}, P_{exp}, RR, and I:E) into the UI, which was then transmitted to the Arduino IDE for display on the serial monitor. Conversely, the output sensor data, including inspiration and expiration pressures, temperature (Temp), and time, was collected by the microcontroller and derived from the counters responsible for valve control. The results from the Arduino serial monitor are presented in **Supplementary Figure S5**. The communication and UI subsystems were integrated to achieve full system functionality, with the test results shown in Figure 12. Figure 12 (a) displays the test for the cyclic mode, while Figure 12 (b) presents the test results for the CNEP mode. On the left aisle of the UI screen, we present the input and output parameters, namely P_{insp}, P_{exp}, RR, I:E, and Temp, accompanied by their respective standard units. On the right side, we showcase the control buttons for alarms and control systems. Additionally, there are control knobs available for adjusting or modifying the input parameters according to the patient's scenario. Positioned at the center of the screen is the pressure plot. Furthermore, the current device mode is displayed at the corner of the screen.

TABLE 6. Comparison of emergency ventilator systems.

Project	Tidal Volume (mL)	Respiratory Rate (bpm)	I:E Ratio	Cost Estimate (USD)
GlasVent [38]	-	-	-	-
MADVent [39]	-	-	-	-
ApolloBVM [97]	300 – 650	5 – 30	1:2 to 1:5	< 300
E-Vent [98]	200 – 800	6 – 40	1:1 to 1:4	~1900
Open-Vent [99]	Max at 800	10 – 30	1:1 to 1:3	-
OxVent [100]	250 – 600	10 – 30	1:1 to 1:3	~1250
Spiro Wave [101]	200 – 800	10 – 35	1:1 to 1:4	-
Umbulizer [102]	200 – 800	1 – 30	1:0 to 1:3	-
AmbuBox [103]	0 – 700	10 – 30	N/A	-
ExoventQ	**0-800**	**10 – 30**	**1:1 to 1:4**	**~1000**

C. TEST OUTCOMES FOR THE SAFETY FEATURES

We tested the alarms from the UI as safety features for both moderate and severe test scenarios, as illustrated in Figure 13. First, we conducted a test for moderate alarms (Figure 13 (a)), where the vessel pressure was allowed to deviate by ± 5 units from the clinician's set pressure. In the case of severe alarms, as depicted in Figure 13 (b), the button's color flashes red, and the buzzer sounds following the alarm limits when the pressure deviates by ± 10 units from the set pressure.

D. COMPARISON TO THE EXISTING VENTILATORS

In response to the global ventilator shortage during COVID-19, innovative low-cost emergency ventilators were developed. ExoventQ, a negative pressure ventilator (NPV), offers a cost-effective solution, overcoming health issues linked to positive pressure ventilators (PPVs). GlasVent prioritizes simplicity and uses 3D-printed parts, suitable for low-resource settings. A closed-loop, pressure-controlled ventilator ensures safety and efficacy. ApolloBVM enhances the Bag Valve Mask with controllable, automated features. The MIT Emergency Ventilator Project automates a manual resuscitator for longer-term use. OpenVent-Bristol proposes a low-tech solution for developing countries. AmbuBox focuses on easy installation, simple operation, and high-precision flow control. Each addresses ventilator shortages uniquely, catering to specific healthcare needs. Table 6 summarizes the comparative analysis of different emergency ventilator systems.

E. LIMITATIONS AND POTENTIAL RISKS

While the study introduces ExoventQ as a novel low-cost portable negative pressure ventilator to address ventilator shortages during COVID-19, it has some potential risks and limitations associated with the device. It is important to thoroughly investigate safety concerns, malfunctions, and adverse events before the clinical trial of this device. While the study briefly mentions safety measures, a more detailed analysis of potential risks and corresponding mitigation strategies is warranted. Additionally, factors such as long-term reliability, user training requirements, and real-world performance challenges should be explored to ensure a thorough understanding of the device's limitations and safety considerations in diverse healthcare settings. Addressing these aspects is crucial for the device's successful integration into clinical practice and for ensuring patient safety.

V. CONCLUSION AND FUTURE WORK

The shortage of ventilators during the COVID-19 pandemic drew public attention to the need for a safe, cost-effective ventilator solution that could be rapidly manufactured to save lives. The potential to save lives among COVID-19 and similar disease patients through the development of an affordable ventilator inspired the creation of **ExoventQ**. The primary innovation of this design lies in its use of Negative Pressure Ventilation (NPV), as opposed to the Positive Pressure Ventilators (PPVs) currently in use in hospitals worldwide, which pose significant health risks in COVID-like scenarios. Furthermore, this study discusses and compares both old and new implementations of NPV, with the best option serving as the basis for the **ExoventQ**design. The vessel underwent significant improvements, transitioning from an initial prismatic shape to a squircle-shaped PC vessel. This vessel was connected to a vacuum cleaner's motor-blower to create a vacuum and featured a closed-loop control system that used feedback from a pressure sensor to regulate the pressure within. The pressure sensor was meticulously calibrated and validated against a handmade manometer, and various temperature sensors were evaluated, with the DHT22 proving the most effective. Motor control and valve control methods were compared, ultimately favoring automatic outflow valve control. The actuator responsible for moving the valve is a servomotor, chosen primarily for its precise rotation angle tracking capability, which could serve as feedback for the closed-loop system. User input for required parameters was facilitated through a Raspberry Pi (RPI) 7-inch touchscreen displaying a user-friendly interface. This interface allowed users to configure different parameters and settings, while data collected from sensors by a microcontroller was conveniently displayed. Additionally, a safety system was integrated, triggering a visual color change and alarm sound when pressure moderately or severely deviated from the preset levels. However, it's important to note that despite the progress made in this study, the **ExoventQ** prototype has several limitations. Since the device couldn't undergo testing on humans in this phase, as it is considered a beta model, testing was conducted using human mannequins to evaluate neck and torso seals. Unfortunately, these mannequins are quite costly, preventing a thorough examination of their impact on pressure within the vessel. Future studies will need to encompass not only technical aspects but also clinical considerations to develop a more robust solution for critically ill patients.

ACKNOWLEDGMENT

The authors would like to acknowledge the guidance and technical support provided in the development phase of the project from Exovent, U.K. The statements made in this

publication are the sole responsibility of the authors. The open-access publication costs have been generously covered by Qatar National Library.

REFERENCES

[1] Mdedge. (Jun. 8, 2017). *The Global Impact of Respiratory Disease—Second Edition*. Accessed: May 22, 2023. [Online]. Available: https://www.mdedge.com/chestphysician/article/140055/society-news/global-impact-respiratory-disease-second-edition

[2] J. B. West, "The physiological challenges of the 1952 Copenhagen poliomyelitis epidemic and a renaissance in clinical respiratory physiology," *J. Appl. Physiol.*, vol. 99, no. 2, pp. 424–432, Aug. 2005, doi: 10.1152/japplphysiol.00184.2005.

[3] WHO. (2022). *WHO Coronavirus (COVID-19) Dashboard*. Accessed: Feb. 2, 2023. [Online]. Available: https://covid19.who.int/

[4] M. Ali, A. R. G. de Azevedo, M. T. Marvila, M. I. Khan, A. M. Memon, F. Masood, N. M. Y. Almahbashi, M. K. Shad, M. A. Khan, R. Fediuk, R. Timokhin, A. Borovkov, and I. U. Haq, "The influence of COVID-19-induced daily activities on health parameters—A case study in Malaysia," *Sustainability*, vol. 13, no. 13, p. 7465, Jul. 2021, doi: 10.3390/su13137465.

[5] M. J. Butler, J. H. Best, S. V. Mohan, J. A. Jonas, L. Arader, and J. Yeh, "Mechanical ventilation for COVID-19: Outcomes following discharge from inpatient treatment," *PLoS ONE*, vol. 18, no. 1, 2023, Art. no. e0277498, doi: 10.1371/journal.pone.0277498.

[6] (2023). *CDC.Gov*. Accessed: Sep. 20, 2023. [Online]. Available: https://www.cdc.gov/

[7] (2020). *CNBC.Com*. Accessed: Sep. 20, 2023. [Online]. Available: https://www.cnbc.com/2020/03/27/trump-orders-general-motors-to-make-ventilators-under-defense-production-act.html

[8] P. A. Drinker, "The iron lung: First practical means of respiratory support," *J. Amer. Med. Assoc.*, vol. 255, no. 11, p. 1476, Mar. 1986, doi: 10.1001/jama.1986.03370110098030.

[9] G. S. Bause, "Emerson respirator or 'iron lung,'" *Anesthesiology*, vol. 110, no. 4, p. 812, Apr. 2009, doi: 10.1097/01.anes.0000348448.45464.e2.

[10] I. Potchileev, M. Doroshenko, and A. N. Mohammed, *Positive Pressure Ventilation*. Treasure Island, FL, USA: StatPearls, 2023. [Online]. Available: https://www.statpearls.com/

[11] C. H. M. Woollam, "The development of apparatus for intermittent negative pressure respiration (2) 1919–1976, with special reference to the development and uses of cuirass respirators," *Anaesthesia*, vol. 31, no. 5, pp. 666–685, Jun. 1976, doi: 10.1111/j.1365-2044.1976.tb11849.x.

[12] R. M. Kacmarek, "The mechanical ventilator: Past, present, and future," *Respiratory Care*, vol. 56, no. 8, pp. 1170–1180, Aug. 2011, doi: 10.4187/respcare.01420.

[13] I. A. Campbell, A. Hill, H. Middleton, M. Momen, and R. J. Prescott, "Intermittent positive-pressure breathing," *BMJ*, vol. 1, no. 6121, p. 1186, 1978.

[14] D. J. Pierson, "Complications associated with mechanical ventilation," *Crit. Care Clinics*, vol. 6, no. 3, pp. 711–724, Jul. 1990, doi: 10.1016/s0749-0704(18)30362-2.

[15] D. Bohn, "The history of high-frequency ventilation," *Respiratory Care Clinics North Amer.*, vol. 7, no. 4, pp. 535–548, Dec. 2001, doi: 10.1016/s1078-5337(05)70005-8.

[16] A. S. Newsome, D. B. Chastain, P. Watkins, and W. A. Hawkins, "Complications and pharmacologic interventions of invasive positive pressure ventilation during critical illness," *J. Pharm. Technol.*, vol. 34, no. 4, pp. 153–170, 2018, doi: 10.1177/8755122518766594.

[17] H. E. Fessler and D. R. Hess, "Respiratory controversies in the critical care setting. Does high-frequency ventilation offer benefits over conventional ventilation in adult patients with acute respiratory distress syndrome?" *Respiratory Care*, vol. 52, no. 5, pp. 595–605, 2007.

[18] W. Clinkscales, M. Spence, J. Gleysteen, N. Hayes, E. Izaguirre, D. Wakefield, D. Schwartz, I. Rhea, C. Risquez, and A. M. Sharma, "Novel use of biphasic cuirass ventilation during definitive radiation therapy: A technical report," *Practical Radiat. Oncol.*, vol. 11, no. 3, pp. e276–e281, May 2021, doi: 10.1016/j.prro.2020.08.003.

[19] S. Takeda, K. Nakanishi, T. Takano, G. Ishikawa, and R. Ogawa, "Effect of external high-frequency oscillation on severe cardiogenic pulmonary edema," *J. Anesthesia*, vol. 11, no. 2, pp. 83–87, Jun. 1997, doi: 10.1007/bf02480066.

[20] J. M. Oropello, V. Kvetan, and S. M. Pastores, *Lange Critical Care*. New York, NY, USA: McGraw-Hill, 2016.

[21] C.-T. Huang, H.-H. Lin, S.-Y. Ruan, M.-S. Lee, Y.-J. Tsai, and C.-J. Yu, "Efficacy and adverse events of high-frequency oscillatory ventilation in adult patients with acute respiratory distress syndrome: A meta-analysis," *Crit. Care*, vol. 18, no. 3, p. R102, 2014, doi: 10.1186/cc13880.

[22] D. M. Linton, "Cuirass ventilation: A review and update," *Crit. Care Resuscitation*, vol. 7, no. 1, pp. 22–28, Mar. 2005.

[23] M. G. Dilkes, A. C. Hill, P. McKelvie, J. M. McNeill, P. S. Monks, and R. G. Hollamby, "The Hayek oscillator: A new method of ventilation in microlaryngeal surgery," *Ann. Otol., Rhinology Laryngol.*, vol. 102, no. 6, pp. 455–458, Jun. 1993, doi: 10.1177/000348949310200609.

[24] A. I. Abboudi, A. I. Alhammadi, K. M. Albastaki, N. U. M. Khanum, and A. Jarndal, "Design and implementation of portable emergency ventilator for COVID-19 patients," in *Proc. Adv. Sci. Eng. Technol. Int. Conf. (ASET)*, Dubai, United Arab Emirates, Feb. 2022, pp. 1–4, doi: 10.1109/ASET53988.2022.9734315.

[25] J. N. Unterborn and N. S. Hill, "Options for mechanical ventilation in neuromuscular diseases," *Clinics Chest Med.*, vol. 15, no. 4, pp. 765–781, Dec. 1994, doi: 10.1016/S0272-5231(21)00968-0.

[26] Y. Sutherasan et al., "Management and outcome of mechanically ventilated patients after cardiac arrest," *Crit. Care*, vol. 19, no. 1, Dec. 2015, doi: 10.1186/s13054-015-0922-9.

[27] C. E. Barrett, J. Park, L. Kompaniyets, J. Baggs, Y. J. Cheng, P. Zhang, G. Imperatore, and M. E. Pavkov, "Intensive care unit admission, mechanical ventilation, and mortality among patients with type 1 diabetes hospitalized for COVID-19 in the U.S." *Diabetes Care*, vol. 44, no. 8, pp. 1788–1796, Aug. 2021, doi: 10.2337/dc21-0604.

[28] H. Hummler and A. Schulze, "New and alternative modes of mechanical ventilation in neonates," *Seminars Fetal Neonatal Med.*, vol. 14, no. 1, pp. 42–48, Feb. 2009, doi: 10.1016/j.siny.2008.08.006.

[29] E. Mireles-Cabodevila, E. Diaz-Guzman, G. A. Heresi, and R. L. Chatburn, "Alternative modes of mechanical ventilation: A review for the hospitalist," *Cleveland Clinic J. Med.*, vol. 76, no. 7, pp. 417–430, Jul. 2009, doi: 10.3949/ccjm.76a.08043.

[30] B. K. Patel, J. P. Kress, and J. B. Hall, "Alternatives to invasive ventilation in the COVID-19 pandemic," *J. Amer. Med. Assoc.*, vol. 324, no. 1, p. 43, Jul. 2020, doi: 10.1001/jama.2020.9611.

[31] J. C. Winck and N. Ambrosino, "COVID-19 pandemic and non invasive respiratory management: Every Goliath needs a David. An evidence based evaluation of problems," *Pulmonology*, vol. 26, no. 4, pp. 213–220, Jul. 2020, doi: 10.1016/j.pulmoe.2020.04.013.

[32] M. V. P. Charles et al., "Ventilator-associated pneumonia," *Australas. Med. J.*, vol. 7, no. 8, pp. 334–344, 2014, doi: 10.4066/AMJ.2014.2105.

[33] U. Khurshid, A. Mahmoud, A. Abducarim, S. Mahmud, O. Abdallah, E. Mohamed, F. Bensaali, A. Amira, A. Alsalemi, A. A. Hssain, G. Alinier, and I. Hassan, "Towards the design and implementation of a human circulatory system for extracorporeal membrane oxygenation simulation," *Egyptian J. Crit. Care Med.*, vol. 6, no. 3, pp. 87–89, Dec. 2018, doi: 10.1016/j.ejccm.2018.12.017.

[34] A. Mahmoud, A. A. Hssain, G. Alinier, I. Hassan, U. Khurshid, A. Abducarim, S. Mahmud, O. Abdallah, E. Mohamed, A. Alsalemi, F. Bensaali, and A. Amira, "Preliminary implementation of the next generation cannulation simulator," in *Proc. IEEE Student Conf. Res. Develop. (SCOReD)*, Oct. 2019, doi: 10.1109/SCORED.2019.8896240.

[35] A. Mahmoud, U. Khurshid, A. Abducarim, S. Mahmud, O. Abdallah, E. Mohamed, A. Alsalemi, F. Bensaali, A. Amira, A. A. Hssain, G. Alinier, and I. Hassan, "Towards next generation cannulation simulators," *Qatar Med. J.*, vol. 2019, no. 2, Feb. 2020, doi: 10.5339/qmj.2019.qccc.61.

[36] S. Jackson, "Ventilator-associated pneumonia in ICU patients with severe pneumonia and respiratory failure," *J. Clin. Invest.*, vol. 133, no. 12, Jun. 2023, doi: 10.1172/jci172643.

[37] C. A. Gao, N. S. Markov, T. Stoeger, A. Pawlowski, M. Kang, P. Nannapaneni, R. A. Grant, C. Pickens, J. M. Walter, J. M. Kruser, L. Rasmussen, D. Schneider, J. Starren, H. K. Donnelly, A. Donayre, Y. Luo, G. R. S. Budinger, R. G. Wunderink, A. V. Misharin, and B. D. Singer, "Machine learning links unresolving secondary pneumonia to mortality in patients with severe pneumonia, including COVID-19," *J. Clin. Invest.*, vol. 133, no. 12, Jun. 2023, doi: 10.1172/jci170682.

[38] A. Christou, M. Ntagios, A. Hart, and R. Dahiya, "GlasVent—The rapidly deployable emergency ventilator," *Global Challenges*, vol. 4, no. 12, Dec. 2020, Art. no. 2000046, doi: 10.1002/gch2.202000046.

[39] A. Vasan, R. Weekes, W. Connacher, J. Sieker, M. Stambaugh, P. Suresh, D. E. Lee, W. Mazzei, E. Schlaepfer, T. Vallejos, J. Petersen, S. Merritt, L. Petersen, and J. Friend, "MADVent: A low-cost ventilator for patients with COVID-19," *Med. Devices Sensors*, vol. 3, no. 4, Aug. 2020, doi: 10.1002/mds3.10106.

[40] (2019). *ISO 19223:2019*. Accessed: May 22, 2023. [Online]. Available: https://www.iso.org/standard/51164.html

[41] E. P. Radford, "Ventilation standards for use in artificial respiration," *J. Appl. Physiol.*, vol. 7, no. 4, pp. 451–460, Jan. 1955, doi: 10.1152/jappl.1955.7.4.451.

[42] K. I. Norton, "Standards for anthropometry assessment," in *Kinanthropometry and Exercise Physiology*, 4th ed., R. G. Eston, Ed. New York, NY, USA: Routledge, 2018, pp. 68–137, doi: 10.4324/9781315385662-4.

[43] Cancer.Gov. (2023). *Mechanics of Ventilation*. Accessed: May 22, 2023. [Online]. Available: https://training.seer.cancer.gov/anatomy/respiratory/mechanics.html

[44] (2023). *Boyle's Law*. Accessed: May 22, 2023. [Online]. Available: https://www.grc.nasa.gov/www/k-12/rocket/boyle.html

[45] G. W. Jenkins, C. Kemnitz, and G. J. Tortora, *Anatomy and Physiology: From Science to Life*, 3rd ed. Nashville, TN, USA: Wiley, 2013.

[46] M. A. Grippi, J. A. Elias, J. Fishman, R. M. Kotloff, A. I. Pack, and R. M. Senior, *Fishman's Pulmonary Diseases and Disorders*. New York, NY, USA: McGraw-Hill Education, 2015.

[47] J. E. Hall, *Guyton and Hall Textbook of Medical Physiology*. Philadelphia, PA, USA: Saunders Elsevier, 2011.

[48] Exovent Development Group, "Exovent: A study of a new negative-pressure ventilatory support device in healthy adults," *Anaesthesia*, vol. 76, no. 5, pp. 623–628, 2021, doi: 10.1111/anae.15350.

[49] F. Cavaliere, G. Conti, R. Costa, G. Spinazzola, R. Proietti, A. Sciuto, and S. Masieri, "Exposure to noise during continuous positive airway pressure: Influence of interfaces and delivery systems," *Acta Anaesthesiologica Scandinavica*, vol. 52, no. 1, pp. 52–56, Jan. 2008, doi: 10.1111/j.1399-6576.2007.01474.x.

[50] R. Al-Humaid. (2018). *Physiology of Lung Volumes and Capacities*. Accessed: May 22, 2023. [Online]. Available: https://www.slideshare.net/RayanSaleh1/physiology-of-lung-volumes-and-capacities

[51] H. Tanaka, T. Yukioka, Y. Yamaguti, S. Shimizu, H. Goto, H. Matsuda, and S. Shimazaki, "Surgical stabilization of internal pneumatic stabilization? A prospective randomized study of management of severe flail chest patients," *J. Trauma, Injury, Infection, Crit. Care*, vol. 52, no. 4, pp. 727–732, Apr. 2002.

[52] D. M. Needham, R. Korupolu, J. M. Zanni, P. Pradhan, E. Colantuoni, J. B. Palmer, R. G. Brower, and E. Fan, "Early physical medicine and rehabilitation for patients with acute respiratory failure: A quality improvement project," *Arch. Phys. Med. Rehabil.*, vol. 91, no. 4, pp. 536–542, Apr. 2010, doi: 10.1016/j.apmr.2010.01.002.

[53] M. Borelli, A. Benini, T. Denkewitz, C. Acciaro, G. Foti, and A. Pesenti, "Effects of continuous negative extrathoracic pressure versus positive end-expiratory pressure in acute lung injury patients," *Crit. Care Med.*, vol. 26, no. 6, pp. 1025–1031, Jun. 1998, doi: 10.1097/00003246-199806000-00021.

[54] R. Kitsommart, K. Nakornchai, B. Yangthara, R. Jiraprasertwong, and B. Paes, "Positive end-expiratory pressure during resuscitation at birth in very-low birth weight infants: A randomized-controlled pilot trial," *Pediatrics Neonatol.*, vol. 59, no. 5, pp. 448–454, Oct. 2018, doi: 10.1016/j.pedneo.2017.12.002.

[55] L. Böttinger and J. W. A. van der Hoorn, "Negative pressure ventilation: A special application of expiratory ventilation assistance," *Intensive Care Med. Exp.*, vol. 7, no. 1, 2019, doi: 10.1186/s40635-019-0248-z.

[56] J. S. Tecklin, "The patient with ventilatory pump dysfunction/failure-preferred practice pattern 6E," in *Cardiopulmonary Physical Therapy*. Amsterdam, The Netherlands: Elsevier, 2004, pp. 344–371, doi: 10.1016/B978-032301840-1.50018-9.

[57] J. M. Gere and B. J. Goodno, *Mechanics of Materials*, 8th ed. Mason, OH, USA: Cengage Learning Custom, 2012.

[58] N. Abughanam, S. S. M. Gaben, M. E. H. Chowdhury, and A. Khandakar, "Investigating the effect of materials and structures for negative pressure ventilators suitable for pandemic situation," *Emergent Mater.*, vol. 4, no. 1, pp. 313–327, Feb. 2021, doi: 10.1007/s42247-021-00181-x.

[59] Ansys. (2023). *Engineering Simulation Software*. Accessed: May 29, 2023. [Online]. Available: https://www.ansys.com/

[60] T. Axsom. (Feb. 17, 2023). *Engineering Fundamentals Refresh: Strength vs. Stiffness vs. Hardness*. Fictiv. Accessed: Sep. 21, 2023. [Online]. Available: https://www.fictiv.com/articles/engineering-fundamentals-refresh-strength-vs-stiffness-vs-hardness

[61] *Young's Modulus, Tensile Strength and Yield Strength Values for Some Materials*. Accessed: Nov. 18, 2023. [Online]. Available: https://www.engineeringtoolbox.com/young-modulus-d_417.html

[62] ACAAI Public Website. *Latex Allergy | Causes, Symptoms & Treatment | ACAAI Public Website*. Accessed: May 29, 2023. [Online]. Available: https://acaai.org/allergies/allergic-conditions/latex-allergy/

[63] Custom Gasket Manuf. LLC. (Sep. 2, 2020). *Neoprene Gasket Material—Properties, Types & Applications*. Accessed: Sep. 21, 2023. [Online]. Available: https://www.customgasketmfg.com/blog/neoprene-gasket-material/

[64] Fire Ice. (2023). *What's an HVAC Blower Motor & Why is It Important?*. Accessed: Sep. 21, 2023. [Online]. Available: https://indoortemp.com/resources/HVAC-blower-motor

[65] Tesla. *Induction Versus DC Brushless Motors*. Accessed: May 29, 2023. [Online]. Available: https://www.tesla.com/blog/induction-versus-dc-brushless-motors

[66] Oriental Motor U.S.A. Corp. *Brushless DC Motor vs. AC Motor vs. Brushed Motor*. Accessed: May 29, 2023. [Online]. Available: https://www.orientalmotor.com/brushless-dc-motors-gear-motors/technology/AC-brushless-brushed-motors.html

[67] Gardner-Denver. *Four Main Types of Blowers*. Accessed: May 29, 2023. [Online]. Available: https://www.gardnerdenver.com/en-qa/knowledge-hub/articles/main-blower-types

[68] LuLu Hypermarket Qatar Website. *Samsung Vacuum Cleaner VC20M2510 2000W Online At Best Price | Canister Vac.Cleaner | Lulu Qatar*. Accessed: May 29, 2023. [Online]. Available: https://www.luluhypermarket.com/en-qa/samsung-vacuum-cleaner-vc20m2510-???2000w/p/1282640

[69] Tameson. *Gate Valve vs Butterfly Valve*. Accessed: May 29, 2023. [Online]. Available: https://tameson.com/pages/gate-valve-vs-butterfly-valve

[70] ThomasNet. *All About Piston Valves*. Accessed: May 29, 2023. [Online]. Available: https://www.thomasnet.com/articles/pumps-valves-accessories/all-about-piston-valves/

[71] (2023). *Electrical4u.Com*. Accessed: Sep. 22, 2023. [Online]. Available: https://www.electrical4u.com/control-system-closed-loop-open-loop-control-system/

[72] M. Inghammar and J. Sunden-Cullberg, "Prognostic significance of body temperature in the emergency department vs the ICU in patients with severe sepsis or septic shock: A nationwide cohort study," *PLoS ONE*, vol. 15, no. 12, Dec. 2020, Art. no. e0243990, doi: 10.1371/journal.pone.0243990.

[73] *Manometer—An Overview | ScienceDirect Topics*. Accessed: May 29, 2023. [Online]. Available: https://www.sciencedirect.com/topics/earth-and-planetary-sciences/manometer

[74] *2.2 The Atmosphere's Pressure Structure: Hydrostatic Equilibrium | METEO 300: Fundamentals of Atmospheric Science*. Accessed: May 29, 2023. [Online]. Available: https://www.e-education.psu.edu/meteo300/node/7

[75] G. Elert, "Density," in *The Physics Hypertextbook*, 2023. [Online]. Available: https://physics.info/

[76] X. Shi, X. Wang, L. Zhang, and K. Guo, "Influence factors of gravitational acceleration near the Earth," *J. Phys., Conf. Ser.*, vol. 1865, no. 2, Apr. 2021, Art. no. 022014, doi: 10.1088/1742-6596/1865/2/022014.

[77] Adafruit Industries. *DHT22 Temperature-Humidity Sensor + Extras*. Unique Fun DIY Electron., Kits. Accessed: May 29, 2023. [Online]. Available: https://www.adafruit.com/product/38

[78] Adafruit Industries. (2023). *DHT11 Basic Temperature-humidity Sensor + Extras*. Unique Fun DIY Electron., Kits. Accessed: May 29, 2023. [Online]. Available: https://www.adafruit.com/product/386

[79] LM35 Data Sheet. *LM35 Data Sheet, Product Information and Support | TI.com*. Accessed: May 29, 2023. [Online]. Available: https://www.ti.com/product/LM35

[80] PowermotionTech. *StackPath*. Accessed: May 29, 2023. [Online]. Available: https://www.powermotiontech.com/hydraulics/hydraulic-pumps-motors/article/21881443/pump-control-vs-valve-control-efficiency-or-performance
[81] P. C. B. Ray. *Fundamental Analysis of DC Stepper VS Servo Motors*. Printed Circuit Board Manuf. PCB Assembly—RayMing. Accessed: May 29, 2023. [Online]. Available: https://www.raypcb.com/dc-stepper-vs-servo-motors/
[82] J. Tang. *The Choice Between Servo Motors and Stepper Motors*. Orientalmotor. Accessed: May 29, 2023. [Online]. Available: https://blog.orientalmotor.com/the-choice-between-servo-motors-and-stepper-motors
[83] Helen. (Apr. 1, 2019). *DC Motor vs Stepper Motor vs Servo Motor—Which to Choose*. Latest Open Tech From Seeed. Accessed: May 29, 2023. [Online]. Available: https://www.seeedstudio.com/blog/2019/04/01/choosing-the-right-motor-for-your-project-dc-vs-stepper-vs-servo-motors/
[84] *HS-646WP High Voltage, High Torque, Analog Waterproof Servo | HITEC RCD USA*. Accessed: May 29, 2023. [Online]. Available: https://hitecrcd.com/products/servos/digital/waterproof-digital/hs-646wp/product
[85] *Exovent | Supporting Negative Pressure Ventilation for Breathing Assistance*. Accessed: May 29, 2023. [Online]. Available: https://exovent.org/
[86] T. Rogers. *Everything You Need to Know About Polylactic Acid (PLA)*. Accessed: May 29, 2023. [Online]. Available: https://www.creativemechanisms.com/blog/learn-about-polylactic-acid-pla-prototypes
[87] Arduino Off. Store. *Arduino Uno Rev3*. Accessed: May 29, 2023. [Online]. Available: https://store.arduino.cc/products/arduino-uno-rev3
[88] Arduin. *Software*. Accessed: May 29, 2023. [Online]. Available: https://www.arduino.cc/en/software
[89] Raspberry Pi Foundation. (Apr. 6, 2023). *Teach, Learn, and Make With the Raspberry Pi Foundation*. Accessed: May 29, 2023. [Online]. Available: https://www.raspberrypi.org/
[90] Raspberry Pi Ltd. *Raspberry Pi OS—Raspberry Pi*. Accessed: May 29, 2023. [Online]. Available: https://www.raspberrypi.com/software/
[91] (Aug. 24, 2021). *What is HTML—Definition and Meaning of Hypertext Markup Language*. Accessed: May 29, 2023. [Online]. Available: https://www.freecodecamp.org/news/what-is-html-definition-and-meaning/
[92] (Apr. 6, 2023). *Cascading Style Sheets*. Accessed: May 29, 2023. [Online]. Available: https://www.w3.org/Style/CSS/Overview.en.html
[93] (2023). *JavaScript Tutorial*. Accessed: May 29, 2023. [Online]. Available: https://www.w3schools.com/js/default.asp
[94] Analog Devices. *UART: A Hardware Communication Protocol Understanding Universal Asynchronous Receiver/Transmitter*. Accessed: May 29, 2023. [Online]. Available: https://www.analog.com/en/analog-dialogue/articles/uart-a-hardware-?communication-protocol.html
[95] W. Storr. (Dec. 12, 2016). *Solid State Relay or Solid-State Switch*. Basic Electron. Tuts. Accessed: May 29, 2023. [Online]. Available: https://www.electronics-tutorials.ws/power/solid-state-relay.html
[96] *Using the Serial Monitor Tool | Arduino Documentation | Arduino Documentation*. Accessed: May 29, 2023. [Online]. Available: https://docs.arduino.cc/software/ide-v2/tutorials/ide-v2-?serial-monitor
[97] *OEDK—Rice University—ApolloBVM*. Accessed: Nov. 19, 2023. [Online]. Available: https://oedk.rice.edu/apollobvm/
[98] *MIT Emergency Ventilator*. Accessed: Nov. 19, 2023. [Online]. Available: https://emergency-vent.mit.edu/
[99] *OpenVent-Bristol*. Accessed: Nov. 19, 2023. [Online]. Available: https://openventbristol.co.uk/
[100] R. Beale et al., "OxVent: Design and evaluation of a rapidly-manufactured COVID-19 ventilator," *eBioMedicine*, vol. 76, Feb. 2022, Art. no. 103868, doi: 10.1016/j.ebiom.2022.103868.
[101] MIT SOLVE. *Spiro Wave*. Accessed: Nov. 19, 2023. [Online]. Available: https://solve.mit.edu/challenges/health-security-pandemics/solutions/31791
[102] *Umbulizer: A Reliable, Portable, and Low-Cost Ventilator*. Accessed: Nov. 19, 2023. [Online]. Available: https://www.umbulizer.com/
[103] Z. Fang, A. I. Li, H. Wang, R. Zhang, X. Mai, and T. Pan, "AmbuBox: A fast-deployable low-cost ventilator for COVID-19 emergent care," *SLAS Technol.*, vol. 25, no. 6, pp. 573–584, Dec. 2020, doi: 10.1177/2472630320953801.

SHAHD SAMEER MOHAMMED GABEN received the B.Sc. degree in electrical engineering from Qatar University, in 2022. She has one journal article. Her research interests include applied artificial intelligence, optimization, sensors and instrumentation, electronics, and biomedical engineering.

NADA ABUGHANAM received the B.Sc. degree in electrical engineering from Qatar University, where she is currently pursuing the master's degree in computing. She has one journal article and three conference papers. Her research interests include machine learning applications, sensors and instrumentation, and electronics.

NABIL IBTEHAZ received the B.Sc. (Eng.) degree from the Department of Electrical and Electronic Engineering, Bangladesh University of Engineering and Technology, and the M.Sc. degree from the Department of Computer Science and Engineering, Bangladesh University of Engineering and Technology. He is currently pursuing the Ph.D. degree in computer science with Purdue University. Previously, he was a Software Engineer at Samsung Research and Development Institute Bangladesh. His current research interests include computational biology, biomedical image and signal processing, machine learning, and computer vision.

SAKIB MAHMUD (Member, IEEE) received the B.Sc. (Hons.) and M.Sc. degrees in electrical engineering from Qatar University (QU), in June 2020 and May 2023, respectively. As an undergraduate student at QU, he has been a part of two Undergraduate Research Experience Program (UREP) projects funded by Qatar National Research Fund (QNRF). Later on, he was hired for more than five high-impact grants from QU, Hamad Medical Corporation (HMC), and QNRF. Throughout the master's degree, during the last two years, he managed to publish more than 20 peer-reviewed journal articles in high-impact journals (mostly Q1, some Q2). His field of expertise mainly comprises but is not limited to machine learning, biomedical instrumentation, signal processing, image processing, bioinformatics, and 3D modeling. As an undergraduate student, he received the Dean's Award for three consecutive years, from 2016 to 2019.

GHADA AL NOAIMI received the B.Sc. degree in electrical engineering from Qatar University, in 2021. Her research interests include sensors and instrumentation, electronics, and biomedical engineering.

ABDULRAHMAN ALQAHTANI received the B.S. degree in biomedical technology from King Saud University, Riyadh, Saudi Arabia, in 2006, and the M.S. and Ph.D. degrees in biomedical engineering from The University of New South Wales, Sydney, Australia, in 2013 and 2019, respectively. He is currently an Assistant Professor with the Department of Medical Equipment Technology, College of Applied Medical Sciences, Majmaah University, and the Department of Biomedical Technology, College of Applied Medical Sciences, Prince Sattam bin Abdulaziz University. His research interests include computational neuroscience, modeling, and simulation of human body organs, neuroprosthetics, neural engineering, medical microwave imaging, and bioimpedance and artificial intelligence.

AMITH KHANDAKAR (Senior Member, IEEE) received the B.Sc. degree in electronics and telecommunication engineering from North South University, Bangladesh, the master's degree in computing (networking concentration) from Qatar University, in 2014, and the Ph.D. degree in biomedical engineering from UKM, Malaysia, in 2023. He has currently around 100 journal publications, ten book chapters, and three registered patents under his name. His research interests include sensors and instrumentation, electronics, engineering education, biomedical engineering, and machine learning applications.

MUHAMMAD E. H. CHOWDHURY (Senior Member, IEEE) received the Ph.D. degree from the University of Nottingham, U.K., in 2014. He was a Postdoctoral Research Fellow with the Sir Peter Mansfield Imaging Centre, University of Nottingham. He is currently an Assistant Professor with the Department of Electrical Engineering, Qatar University. He has filed several patents and published more than 150 peer-reviewed journal articles, more than 30 conference papers, and several book chapters. He is running NPRP, UREP, and HSREP grants from the Qatar National Research Fund (QNRF) and internal grants (IRCC and HIG) from Qatar University along with academic projects from HBKU and HMC. His current research interests include biomedical instrumentation, signal processing, wearable sensors, medical image analysis, machine learning, computer vision, embedded system design, and simultaneous EEG/fMRI. He is a member of British Radiology, ISMRM, and HBM. He has recently won the COVID-19 Dataset Award, the AHS Award from HMC, and the National AI Competition Awards for contributing to the fight against COVID-19. His team is the gold medalist at the 13th International Invention Fair in the Middle East (IIFME). He serves as the Guest Editor for *Polymers*, an Associate Editor for IEEE Access, and a Topic Editor and a Review Editor for *Frontiers in Neuroscience*. Since 2022, he has been listed among the Top 2% of Scientists in the World List, published by Stanford University.